PERFORMANCE ANALYSIS OF ULTRA WIDEBAND COMMUNICATION SYSTEMS

By

LakshmiNarasimhan SrinivasaRaghavan

A Thesis
Submitted to the
Faculty of the Graduate School
of
Western Carolina University
in Partial Fulfillment of
the Requirements for the Degree
of
Master of Science in Technology

Committee:

_____ Director

_____

_____

_____ Dean of the Graduate School

Date: _____

Spring 2011
Western Carolina University
Cullowhee, North Carolina

PERFORMANCE ANALYSIS OF ULTRA WIDEBAND COMMUNICATION SYSTEMS

A thesis presented to the faculty of the Graduate School of Western Carolina University in partial fulfillment of the requirements for the degree of Master of Science in Technology.

By

LakshmiNarasimhan SrinivasaRaghavan

Director: James Z. Zhang, Ph.D.
Associate Professor
Department of Engineering and Technology

Committee Members:
Dr. Brian Howell, Department of Engineering and Technology
Dr. Yeqin Huang, Department of Engineering and Technology

April 2011

ACKNOWLEDGEMENTS

I am heartily thankful to my thesis director, Dr. James Zhang, whose encouragement, guidance and support from the initial to the final level enabled me to develop an understanding of the subject. I would also like to thank my committee members Dr. Brian Howell and Dr. Yeqin Huang for their assistance and encouragement.

I would like to show my gratitude to all the faculty members of Kimmel School and Criminology and Criminal Justice Department for their support in the data collection campaign. I am indebted to many of my graduate student colleagues for their support.

Lastly, I offer my warmest regards and thanks to my family for their continued support.

TABLE OF CONTENTS

LIST OF TABLES

LIST OF FIGURES

ABSTRACT

PERFORMANCE ANALYSIS OF ULTRA WIDEBAND COMMUNICATION SYSTEMS

LakshmiNarasimhan SrinivasaRaghavan, M.S.T.

Western Carolina University (April 2011)

Director: James Z. Zhang, Ph.D.

Ultra Wideband (UWB) radio is one of the emerging technologies which have promising characteristics such as high data rate transmission, material penetration, multiple access capability and reduced fading. It has the potential to evolve as the future solution to high data rate short range wireless communication, and other applications including imaging and radar.

This research aims to establish a comprehensive database, performance verification of the existing channel models, and a proposal of new channel models. This research contributes further to the channel characterization of the UWB channels and proposes a new model with enhanced statistical description using a large database of indoor and outdoor UWB measurements. The existing channel models are inadequate to study the delay characteristics of the UWB channel. The proposed model has new information regarding statistical descriptions of channel delay characteristics, including mean excess delay and root mean square (RMS) delay spread.

CHAPTER 1: INTRODUCTION

A communication system is said to be Ultra Wide Band (UWB) if the instantaneous spectral occupancy of the system is more than 500MHz or fractional bandwidth is more than 20%. The waveform type used in UWB communication is an ultra short (nanosecond scale) pulse waveform instead of a sinusoidal waveform carrier to carry the data, which facilitates the system to communicate in the UWB frequency range. UWB radio is one of the emerging technologies which has very promising characteristics to evolve as the future solution to the high data rate short range wireless communications, networking, radar, imaging and positioning systems.

There is enormous potential to explore and analyze the UWB system, though the concept of wide-band communication is very old. The 2002 Federal Communication Commission (FCC) regulation to clear the spectrum for commercial deployment of UWB gave an impetus to the research of UWB systems. Prior to the 2002 FCC regulation, UWB research was concentrated on radar systems primarily for military applications. The FCC regulation gave an impetus for other countries, such as Japan, Korea, China and countries in Europe to enact their own respective regulations for UWB deployment.

The unique advantages of the UWB that makes it more attractive are:

- Enhanced capability to penetrate through obstacles.
- Accurate position estimation.

- Multiple-access capability through spread spectrum.
- Reduced fading due to fine multi-path resolution.

Due to the robustness of the UWB system in dense multi-path environment and the ability to transfer date at very high rates ($\geq$600 Mbps) in short distance(5-10m), it is a highly sought communication method for indoor wireless communications. Out of the many UWB applications, this work analyzes the performance of the UWB system for indoor wireless communications. Wireless personal area networks (WPANs) also known as in-home networks address short-range ad hoc connectivity among portable consumer electronic and communication devices. They are envisioned to provide high-quality real-time video and audio distribution, file exchange among storage systems, and cable replacement for home entertainment systems. UWB technology emerges as a promising physical layer candidate for WPANs, because it offers high-rates over short range, with low cost, high power efficiency, and low duty cycle.

An accurate channel model is extremely important for efficient communication system design. The overall channel model for indoor communication is typically broken down into two main components, a ”large scale” and a ”small scale” model. Specifically, large scale models are necessary for network planning and link budget design while small scale models are necessary for efficient receiver design and performance analysis [13]. This thesis examines the pathloss model and indoor channel characteristics of the UWB signals.

Because of the nature of UWB system to have a very wide instantaneous bandwidth and large number of resolvable multipath rays, the traditional narrowband channel models are inadequate to study the UWB system. The traditional channel models were developed for system with bandwidth less than 20MHz. To overcome the limitations, a

comprehensive database is built and UWB channel models can be characterized by applying the statistical methods on the measured empirical data. Several statistical models for UWB channel behavior have been proposed in [9] - [15]. This thesis builds on the exponential decay modeling of the delay profile approach propsed in [12]. The differences in our database are measurement bandwidth and inclusion of different types of layout in the measurement campaign.

The rest of the thesis is organized as follows: The second chapter is background theory or literature review which gives an in-depth understanding of the previous works and their importance to this thesis. The third chapter explains the detailed methodology of the work and the fourth chapter illustrate the results arrived through the work. The final chapter provides conclusion and the future works.

CHAPTER 2: BACKGROUND THEORY

The UWB communication system uses ultra short pulse waveforms for the transmission of data in order to operate in the UWB frequency range and also to comply with the Federal Communication Commission's (FCC) regulation. In general, the transmitted waveform can be mathematically expressed as

$$Y(t) = \Sigma_{n=-\infty}^{\infty} \Psi[t - nT - c_n T_c] \tag{2.1}$$

where $\Psi(t)$ is the transmitted pulse, T is the frame repetition time, c_n is the pseudorandom, repetitive time hopping sequence and T_c is the time hop delay. A commonly used waveform is the second derivative of the Gaussian monopulse which can be represented by

$$\Psi(t) = \sqrt{\frac{4}{3\sigma\sqrt{\pi}}} \left(1 - \frac{t}{\sigma^2}\right) e^{\left(-\frac{1}{2}\frac{t}{\sigma}^2\right)} \tag{2.2}$$

where σ determines the effective time width of the pulse. Using the latter definition, an example of a typical UWB pulse is shown in figure 2.1.

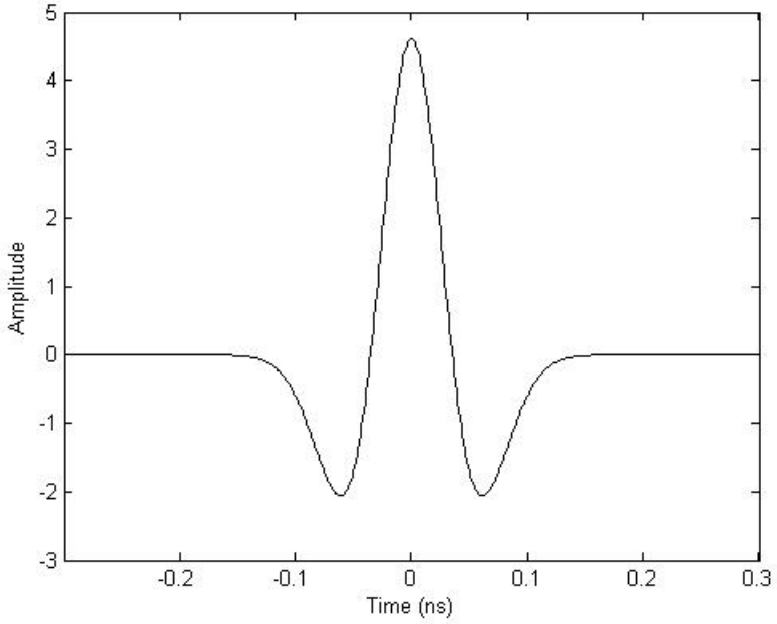

Figure 2.1: A Typical UWB Pulse

The above shown pulse is the ideal gaussian pulse used in the UWB device. But in real time a UWB pulse transmitted through an antenna undergoes a phenomena called ringing due to the extreme high frequency of the pulse. The above shown UWB pulse when transmitted through an antenna start ringing and it resembles a sinusoidal waveform as shown in figure 2.2.

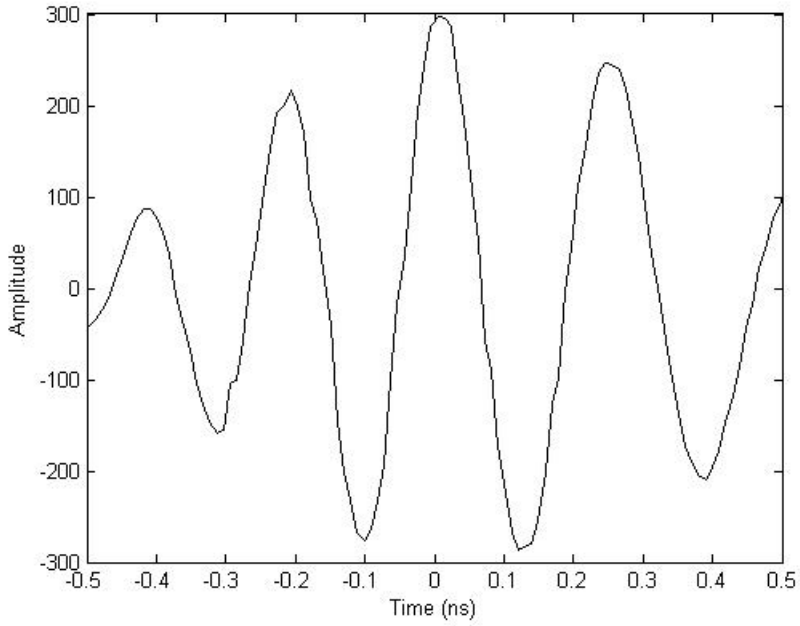

Figure 2.2: Ringing UWB Pulse

The 2002 FCC regulation governs the emissions of the UWB system. It allows the use of UWB devices as long as the system complies with the spectral mask as shown in figure 2.3. For wireless communication in particular, the FCC regulated power levels are very low (below -41.3 dBm), which allows UWB technology to overlay already available services such as the global positioning system (GPS) and the IEEE 802.11 wireless local area networks (WLANs) that coexist in the 3.6 - 10.1 GHz band. Although UWB signals can propagate greater distances at higher power levels, current FCC regulations enable high-rate data transmission over short range at very low power. Similar to the frequency reuse principal exploited by wireless cellular architectures, low power, short-range UWB communications are also potentially capable of providing high spatial capacity, in terms of bits per second per square meter [8].

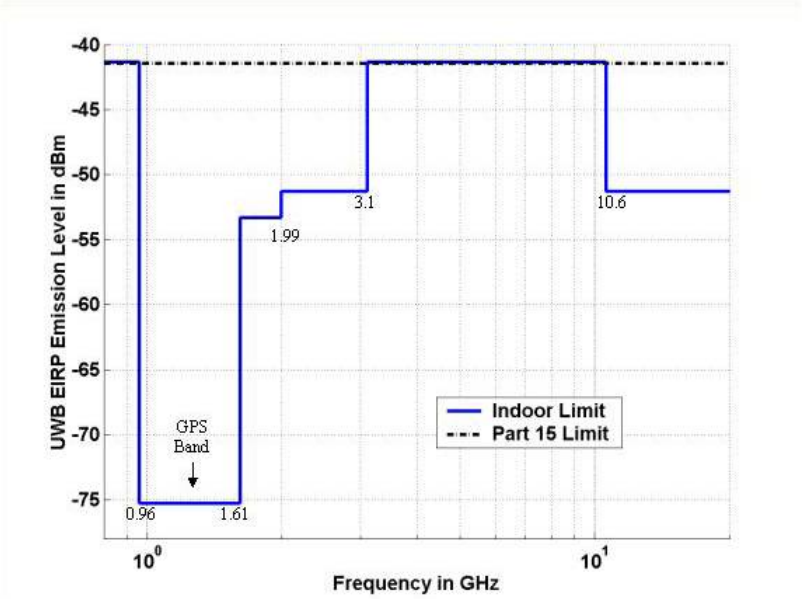

Figure 2.3: Indoor FCC Spectral Mask

Any wireless communication link is subject to noise and attenuation due to many factors. The simplest noise channel is the classical Additive White Gaussian Noise (AWGN), with statistically independent Gaussian noise corrupting data samples, is the usual starting point for understanding basic performance relationships of communication systems. The primary source of performance degradation is thermal noise generated in the receiver. The thermal noise usually has a flat power spectral density over the signal band and a zero-mean Gaussian voltage probability density function [19]. The mathematical representation of the corrupted signal is given by

$$r(t) = Y(t) + n(t) \tag{2.3}$$

where n(t) is the Gaussian noise with power spectral density of $\frac{N_0}{2}$. The attenuation behind electromagnetic wave propagation are diverse, but generally can be attributed to reflection, diffraction, and scattering. Due to multiple reflections from various objects, the electromagnetic waves travel along different paths of varying lengths. The interaction between

these waves causes multipath fading at a specific location, and the strengths of the waves decrease when the distance between transmitter and receiver increases [1]. An example UWB pulse captured in dense multipath environment with different multipath components is shown in figure 2.4

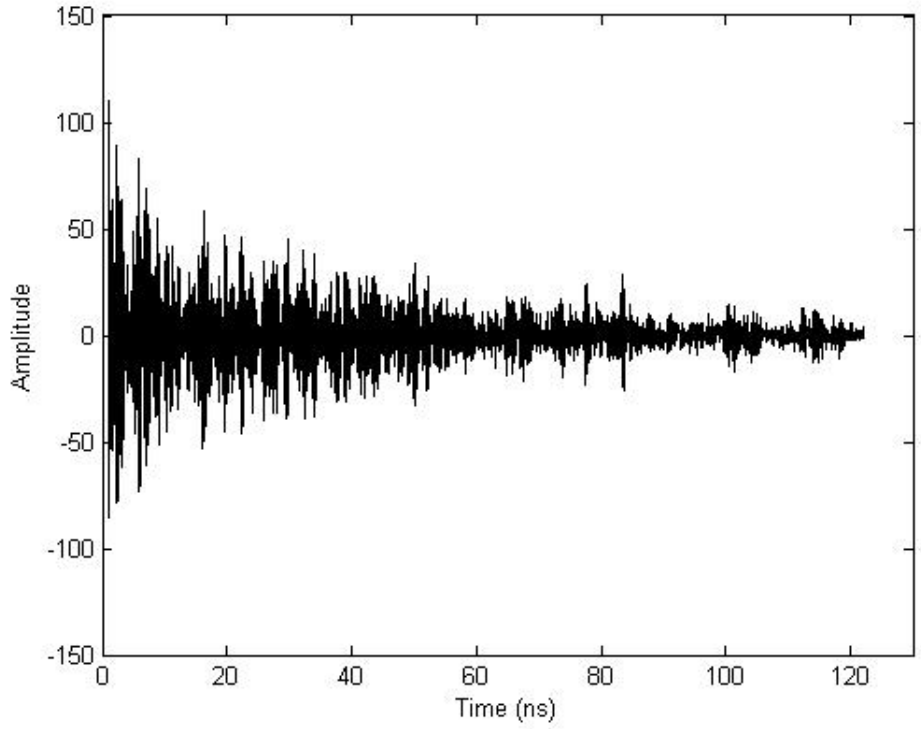

Figure 2.4: A Received UWB Signal

Propagation models have traditionally focused on predicting the average received signal strength at a given distance from the transmitter, as well as the variability of the signal strength in close spatial proximity. Propagation models that predict the mean signal strength at a given distance from the transmitter -receiver (T-R) separation distance are useful in estimating the radio coverage area of the transmitter and are called large-scale propagation models. On the other hand, propagation models that characterize the rapid

fluctuations of the received signal strength over very short travel distance (a few wavelengths) are called small-scale models [1].

2.1 Free Space Propagation

The free space propagation model is used to predict received signal strength when the transmitter and receiver have a clear, unobstructed line-of-sight (LOS) path between them. The free space power received buy the receiver antenna which is separated from a radiating transmitter antenna by a distance d, is given by the Friis free space equation,

$$P_r(d) = \frac{P_t G_t G_r \lambda^2}{(4\pi)^2 d^2 L} \tag{2.4}$$

where P_t is the transmitted power, $P_r(d)$ is the received power which is a function of the T-R separation, G_t is the transmitter antenna gain, G_r is the receiver antenna gain, d is the T-R separation distance in meters, L is the system loss factor not related to propagation, and λ is the wavelength in meters [1]. Formula (2.4) in general states that received signal power decreases with the distance squared. However, it also states that received power decreases with the square of frequency. The extremely large bandwidth of UWB signals, would tend to suggest that the channel will introduce frequency dependent path loss and thus distort the pulse shape. But in [13] it was ascertained that while the receiver power may be dependent on frequency, the path loss is not dependent on frequency. It was also concluded that the frequency dependence is related to the antenna. The received power at the free space, with reference to a reference point d_0 is given by

$$P_r(d) = P_r(d_0) \left(\frac{d_0}{d} \right)^2 \tag{2.5}$$

2.2 Multi-Path Propagation

The propagation mechanisms like reflection, diffraction, and scattering manifests the transmitted signal to multiple waveforms and are called multi-path propagation. These multi-path waves combine at the receiver antenna to give a resultant signal which can vary widely in amplitude and shape, depending on the distribution of the intensity and relative propagation time of the waves and the bandwidth of the transmitted signal resulting in small scale fading [1].

The multipath delay axis τ of the impulse response is discretized into equal time delay segments called excess delay bins, where each bin has a time delay width equal to $\tau_{i+1} - \tau_i$. Any number of multipath signals received within the i^{th} bin are represented by single Resolvable Multipath Component (MPC) having delay τ_i [1]. Despite the high temporal resolution of the UWB systems, there is still an appreciable probability that several MPCs fall into one resolvable delay bin and add up there; in other words there is fading even in UWB. The difference to a conventional system lies mainly in the number of MPCs that fall into a bin. This number is influenced by i)the environment: the more objects are in the environment, the more MPCs can occur; ii) the measurement bandwidth: clearly, a larger bandwidth, and thus a shorter duration of a resolvable delay bin, reduces the number of MPCs per bin; and iii) the delay of the considered bin: for larger excess delay there are more feasible paths causing this particular delay [11].

The small scale variations of a mobile radio signal can be directly related to the impulse response of the mobile radio channel. The impulse response is a wide-band channel characterization and contains all the information necessary to simulate or analyze any type of radio transmission through the channel. Since the received signal in a multipath channel consists of a series of attenuated, time-delayed, phase shifted replicas of the transmitted

signal, the baseband impulse response of a multipath channel can be expressed as

$$h(t,\tau) = \Sigma_{i=0}^{N-1} a_i(t,\tau) e^{j(2\pi f_c \tau_i(t) + \phi_i(t,\tau))} \delta(\tau - \tau_i(t)) \tag{2.6}$$

where τ represents the channel multi-path delay for a fixed value at t, N represents total number of possible multi-path components, $a_i(t,\tau)$ and $\tau_i(t)$ are the real amplitudes and excess delays, respectively, of the i^{th} multipath component at time t. The phase term $2\pi f_c \tau_i(t) + \phi_i(t,\tau)$ represents the phase shift due to free space propagation of the i^{th} multi-path component, plus any additional phase shifts which are encountered in the channel and $\delta(\cdot)$ is the unit impulse function which determines the specific multi-path bins and have components at time t and excess delays τ_i [1].

2.3 Channel Models

There has been a great interest from academia and industry on the research of UWB communication in the past several years. These research interests had a snow ball effect since the early study conducted by Win and Scholtz in the 1990's [2] - [5]. The characterization of the indoor channel model of the UWB system is typically done by statistically characterizing the power delay profile (PDP) of the channel. The PDP of the channel is found by taking the spatial average of $|h(t)|^2$ over a local area.The PDP in given by,

$$p(\tau) = \Sigma_i p_i \delta(\tau - \tau_i);\ \Sigma_i p_i = 1 \tag{2.7}$$

and is uniquely determined by the power delay set p_i, τ_i, where p_i and τ_i are the power and time delay at the i^{th} bin respectively. In a given bandwidth, W, sampling theory tells us that the impulse response (and, by extension, the delay profile) is completely determined by a set of samples spaced by $\frac{1}{W}$ or less. Therefore, one way to characterize a PDP is via a set of samples spaced by $\frac{1}{W}$ (i.e., $\tau_i = \frac{i}{W}, i = 0,1,2,\ldots$), and the result is suitable for any

bandwidth of W or smaller. Alternatively, one can model the physical multipath echoes, which may arrive at arbitrary delays bearing no relationship to integer multiples of $\frac{1}{W}$. The delay profile model is required to have the following three parts [17]:

1. A functional description of power vs. delay.
2. A set of probability distributions for those function parameters that vary across T-R paths and/or buildings.
3. A set of numerical values for both the function parameters that are fixed and the parameters of the probability distributions.

In order to compare different channels and to develop some general design guidelines for wireless systems, parameters which grossly quantify the multipath channel are used. The mean excess delay and root mean square (rms) delay spread that can be determined by the power delay profile. The time dispersive properties of wideband multipath channels are most commonly quantified by their mean excess delay ($\overline{\tau}$) and rms delay spread (τ_{rms}). The mean excess delay is the first moment of the power delay profile and is defined as [1]

$$\overline{\tau} = \frac{\Sigma_k p(\tau_k)\tau_k}{\Sigma_k p(\tau_k)} \tag{2.8}$$

The rms delay spread is the square root of the second central moment of the power delay profile and is defined as

$$\tau_{rms} = \sqrt{\overline{\tau^2} - (\overline{\tau})^2} \tag{2.9}$$

where

$$\overline{\tau^2} = \frac{\Sigma_k p(\tau_k)\tau_k^2}{\Sigma_k p(\tau_k)} \tag{2.10}$$

Although there has been a considerable amount of research activity on the characterization of the UWB channels, three most predominant channel models are investigated

and presented below. The notations and description in expressing all the power delay profiles are modified to be uniform across the three models for greater clarity as given in [17].

2.3.1 Exponential Model

The modeling approach in [12] is based on the investigation of the statistical properties of the multipath profiles measured in different rooms over finely spaced measurement grid. The analysis leads to the formulation of the a stochastic tapped-delay-line (STDL) model of the UWb indoor channel. The PDP as a function of delay, τ, is represented by discrete samples spaced by $\frac{1}{W}$, where the first term has a relative amplitude of 1; and all subsequent terms decay with τ as $\frac{1}{W}$- spaced samples of the decaying exponential $re^{(-\tau/\varepsilon)}$. where τ and the time constant, ε are in ns. Thus, the two parameters that define a given PDP are r (the ratio of the second term to the first) and ε (the decay "time constant" for all terms following the first). The exponential decay is truncated at $\tau = 5\varepsilon$. Referring to (2.7), we can say that $\tau_i = i/W$, and

$$p_i = \begin{cases} c, & \tau_i = 0 \\ cre^{-\tau_i/\varepsilon}, & 0 < \tau_i \leq 5\varepsilon \end{cases} \tag{2.11}$$

where c is a normalizing constant chosen to make the sum of the p_i's unity.

The structure of this PDP model includes specifying how r and ε are distributed over T-R paths. The assumption made is that both are lognormal, i.e., $10\log_{10} r$ and $10\log_{10}\varepsilon$ are both Gaussian random variates over the population of all possible T-R paths. The numerics of the model consist of specifying the mean and standard deviation of these decibel quantities. The means were -4 and -16.1, respectively, while the standard deviations were 3 and 1.27, respectively.

The total average power $\overline{p}_{tot}$ within each room is obtained by integrating the local spatial sample points of each room over all delay (τ_i). Because of shadowing phenomenon,

the $\overline{p}_{tot}$ varies lognormally about PL with a standard deviation of the associated normal random variable equal to 4.3. Where PL is given by

$$PL = \begin{cases} 20.4 \cdot log_{10}(d/d_0), & d \leq 11m \\ -56 + 74 \cdot log_{10}(d/d_0), & d > 11m \end{cases} \tag{2.12}$$

Since PDP is the result of local spatial averaging of the squared amplitudes of the impulse response samples, the probability density function (pdf) of the local sample at delay τ is the Gamma distribution, with m-parameter has a truncated Gaussian pdf over all T-R paths, with its mean and variance both linearly decreasing functions of τ.

The database for this model is a set of measurements made in a 500MHz bandwidth using baseband pulses. The measurements were conducted at 14 locations within one office building , with T-R distances ranging from 6 m to 17m. Of the 14 paths measured, two were line-of-sight (LOS) and 12 non line-of-sight (NLOS), and all are statistically modeled as one population. For each receive location, spatial averaging was done over 49 positions using 7×7 grid with spacings of 15cm.

2.3.2 Cluster Model

This is the IEEE 802.15.3a standard delay profile model for UWB personal area networks [9] and is a variation on the Saleh-Valenzuela cluster model devised for narrowband indoor channels. The cluster model is modeled as follows;

1. It has no distinct LOS term at the minimum delay
2. It allows for multiple exponentially decaying sets of samples
3. The impulses in $p(\tau)$ are not uniformly spaced but represent echoes at arbitrary delays dictated by the scatterer geometries.

The PDP for a given T-R path can be expressed as follows:

$$p(\tau) = c\,\Sigma_l |\xi_l|^2\,\Sigma_k\,\overline{|\beta_{k,l}^2|}\,\sigma(\tau - T_l - \tau_{k,l}) \tag{2.13}$$

where l is the cluster index ($l = 0,1,2,\ldots$); k is the ray index within a cluster ($k = 0,1,2,\ldots$); T_l is the delay of the first ray of the l^{th} cluster; $\tau_{k,l}$ is the delay of the k^{th} ray of the l^{th}cluster, measured from $\tau = T_l$; $|\xi_l|^2$ is a scale factor for the l^{th} cluster; $\overline{|\beta_{k,l}|^2}$ is the locally-averaged power of the k^{th} ray of the l^{th} cluster; and c is a normalizing factor that makes the sum of all terms equal to 1. We now elaborate these delays and amplitudes.

- *Cluster Scale Factor*, $|\xi|^2$ - This random factor is independent from cluster to cluster in the same T-R path, and from path to path. It is lognormal, with the dB standard deviation σ_1. It has no local spatial variation.

- *Delays* T_l and $\tau_{k,l}$ - Both the cluster delay, T_l, and the ray delay within the cluster, $\tau_{k,l}$, are assumed to have Poisson statistics, with average arrival rates of Λ and λ, respectively.

- *Ray Amplitude*, $\overline{|\beta_{k,l}|^2}$ - This local spatial average of $\overline{|\beta_{k,l}|^2}$ is of the form

$$\overline{|\beta_{k,l}|^2} \propto e^{\frac{-T_l}{\Gamma}} e^{\frac{-\tau_{k,l}}{\gamma}}, \tag{2.14}$$

  indicating an exponential decay of the cluster amplitudes, with decay "time constant" Γ; and an additional decay of the rays within a cluster, with decay "time constant" γ.

- *Spatial Variation of* $\overline{|\beta_{k,l}^2|}$ - Although we consider only the average of this term, its local spatial variability is modeled as lognormal, with a dB mean of zero and dB standard deviation of σ_2. This is in contrast to the exponential model, [12], wherein a Gamma pdf is used. Moreover, σ_2 is not a function of delay, whereas the

Gamma distribution's m-parameter is, as noted above. The local spatial variation is independent among individual rays.

The model is based on extensive residential measurements over a 6GHz bandwidth centered on 5.0GHz, over distance up to 10m in various environments.

2.3.3 Exponential- Lognormal Model

This model [15], the PDP for NLOS T-R paths varies with delay as a decaying exponential times a noise-like variation that behaves as a correlated lognormal random process. For LOS T-R paths, there is a distinct term at the minimum delay followed by an exponential - lognormal term just like the one for NLOS T-R paths. Thus, in (2.7), $\tau_i = i/W$, and p_i, is given by

$$p_i = \begin{cases} ke^{-\frac{\tilde{\alpha}\tau_i}{\bar{\tau}_{rms}}} s(\tau_i), & i \geq 0 \text{ NLOS} \\ 10^{A/10}, & i = 0 \text{ LOS} \\ ke^{-\frac{\tilde{\alpha}\tau_i}{\bar{\tau}_{rms}}} s(\tau_i), & i > 0 \text{ LOS} \end{cases} \tag{2.15}$$

where $\tilde{\alpha}$ is a dimensionless decay constant, which varies with T-R distance, d; A is the direct (LOS) amplitude, which varies with d; $s(\tau_i)$ is a noise-like variation with delay which, over the ensemble of all T-R paths, behaves like a correlated lognormal process; $\bar{\tau}_{rms}$ is a global average of the rms delay spread; and k is a normalizing factor that causes the sum of all p_i's to be 1.

The function parameters are derived with the decibel (dB) values of p_i, thereby converting the exponential decay into a straight line function of τ_i and the lognormal variation $s(\tau_i)$ to a Gaussian one. This permitted the use of simple linear regression to find the parameters . In the conversion to dB, $\tilde{\alpha}$ and $s(\tau_i)$ are replaced by

$$\alpha = (10/\ln 10)\tilde{\alpha} \tag{2.16}$$

$$S_i = 10\log_{10}(s(\tau_i)) \tag{2.17}$$

The parameters α, A, and S_i are elaborated below:

- *Decay Constant* α - This parameter varies with d according to

$$\alpha = \alpha_0 - \gamma \log_{10}(d) + \varepsilon \quad (d \text{ in meters}) \tag{2.18}$$

where α_0 is a constant; ε is a zero-mean Gaussian random variate from one distance to another, with standard deviation σ_α; and γ is a random variate from building to building, defined by the pdf

$$p(\hat{\gamma}) = \frac{1}{u^v \Gamma(v)} \hat{\gamma}^{v-1} e^{-\hat{\gamma}/u}; \quad \hat{\gamma} = \gamma + 2 \tag{2.19}$$

$$\Gamma(v+1) = \int_0^\infty y^v e^{-y} dy; \quad v > -1 \tag{2.20}$$

where $\Gamma()$ is the Gamma function, and u and v are fitting parameters and positive.

- *LOS Amplitude*, A - This dB amplitude varies with d according to

$$A = A_0 - 10\gamma_A \log_{10}(d) + \varepsilon_A \quad (d \text{ in meters}) \tag{2.21}$$

where A_0 and γ_A are constants; and ε_A is a zero-mean Gaussian random variate from one distance to another, with standard deviation σ_A. The pdf of A is truncated to a maximum value of 0 dB.

- *Lognormal Variation*, $s(\tau_i)$ - The dB value of $s(\tau_i)$, which is called as S_i, is characterized by

$$S_i = \sigma_s \left[\sigma_0 e^{(-\beta_i / W\bar{\tau}_{rms})} \right] x_i; \quad i = 0, 1, 2, \ldots \tag{2.22}$$

where σ_s, σ_0 and β are constants; and x_i is a zero-mean Gaussian sequence with autocorrelation function

$$\rho_x(x) = \begin{cases} 1; & n = 0 \\ a e^{(-|n|b/W\bar{\tau}_{rms})}; & |n > 0| \end{cases} \tag{2.23}$$

where a and b are constants.

All the three models stated above can be specified by their parameter set and can be quantified for different environments for easier comparison. In table 2.1 the parameter sets for all the three channel models are given.

Table 2.1: Delay Profile Model Parameters

Model	Parameter
Exponential	r, ε
Cluster	σ_1, Λ, λ, Γ, γ
Exponential - Lognormal - NLOS	α_0, v, u, σ_ε, A_0, γ_A, σ_A, a, b, σ_S, σ_0, β, $\overline{\tau}_{rms}$
Exponential - Lognormal - LOS	α_0, v, u, σ_ε, a, b, σ_S, σ_0, β, $\overline{\tau}_{rms}$

In [17] the above three models are compared and tested against the database and against each other by computing certain statistical attributes of the ensemble of channel delay profiles. The statistical attributes compared for the above three models are

1. The cumulative distribution function (CDF) of the mean delay, $\overline{\tau}$, across the ensemble.

2. The CDF of the rms delay spread, τ_{rms}, across the ensemble.

3. The mean across the ensemble of $p(\tau)$, denoted by $\mu_p(\tau)$.

4. The standard deviation across the ensemble of $p(\tau)$, denoted by $\sigma_p(\tau)$.

It was shown that each of the modeling approaches yields reasonable agreement with the database for most or all of the attributes tested. In every case, the results for all three models are not dramatically different from those for the database ensemble of PDPs.

CHAPTER 3: EXPERIMENTAL PROCEDURE

3.1 Experimental Setup

One of the goals defined for this thesis is to build a comprehensive database by initiating a data collection campaign. The database should consist of different components like LOS, NLOS data at different layouts and at different raw datarates. The experimental setup devised to accomplish the goal consists of the following elements:

3.1.1 Areas and Locations

An area represents a particular group of locations which represent a layout or an environment. A location represents one of many measuring locations in a given area. The areas were carefully chosen for the data collection to represent a subset of different layouts in academic, residential and industrial environment. In a given area different locations were chosen to include both LOS and NLOS data with varying distance in the database. All the areas were chosen in Belk and CAT buildings which represent the above mentioned environments. The partitions in the areas chosen include both dry and concrete walls. The areas can be broadly classified as follows:

- Academic Environment:

  The academic environment includes galleries with rows of faculty offices and corridors with classrooms and laboratories on either side. The areas with rows of faculty offices are Gallery 340 (figure 3.1a), Gallery 111 (figure 3.1b) and Corridor 103 (figure 3.1c) in Belk building. The other type of layout was Corridor 352 (figure 3.2) in

Belk building with classrooms and laboratories on either side. The total number of locations measured in this environment is 30.

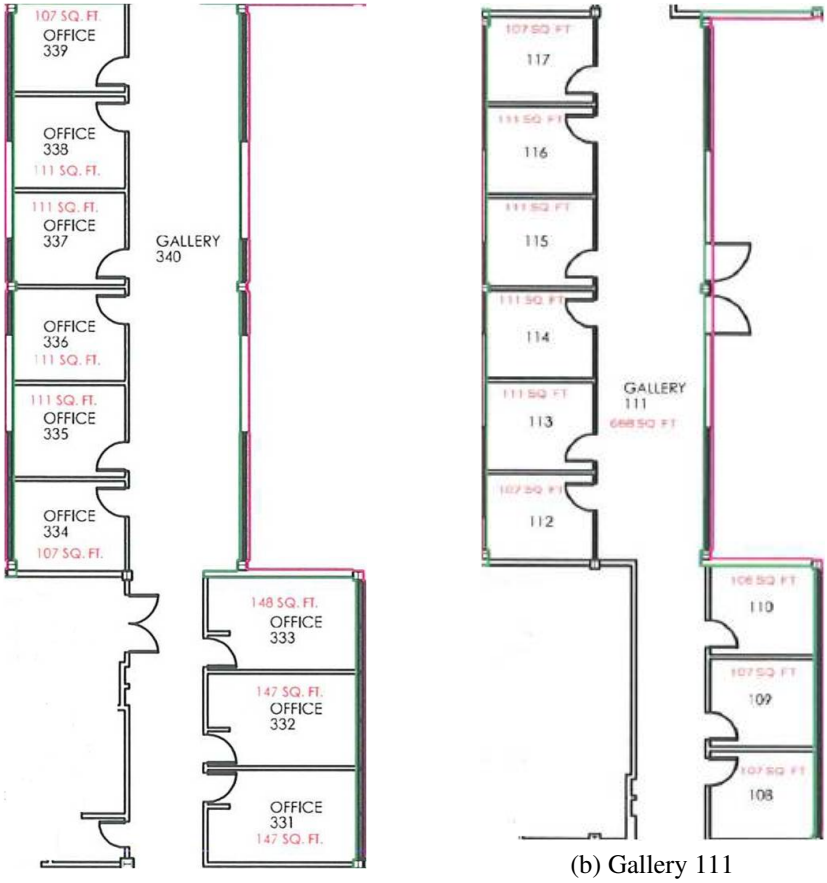

(a) Gallery 340

(b) Gallery 111

(c) Corridor 352

Figure 3.1: Academic Environment - Faculty Offices

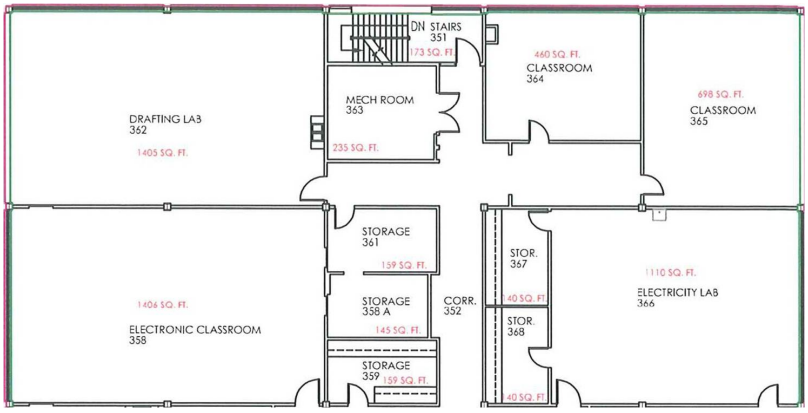

Figure 3.2: Academic Environment - Corridor 352

- Industrial Environment:

  The industrial environment is included in the database by collecting the data in Optics and Telecommunications laboratories in CAT building. Both the laboratories have high ceiling and inconsistent obstructions by the equipments and lab furniture that could imitate an industrial environment while measuring the UWB data. The total number of locations measured were 8 with 4 locations in each lab having a mix of both LOS and NLOS communications.

- Residential Environment:

  A structure similar to a residential environment with a big living room and multiple rooms layout is chosen. The area chosen comes close to duplicate a residential environment. Belk 362 is organized in such a way that there are multiple rooms of comparable sizes surrounding a big room. There was a total of 5 receiver locations where some communication links were LOS and others were NLOS.

- Indoor and Outdoor Pathloss Measurement:

  To calculate the pathloss of the UWB data in both indoor and outdoor LOS environment, two areas were chosen. For the outdoor LOS environment, Intramural field

was chosen and the data measured varied in distance from 3.2m to 60m with 58 measurements taken with each measurement location spaced 1 meter apart. For the indoor environment the hallway in Gallery 340 was chosen with distance varying from 3.2m to 30m, with 28 measurement taken with each measurement location spaced at 1 meter distance.

3.1.2 UWB Radio

The UWB radio used for measurement is a commercially available transceiver UWB radio. All the measurements were made in time domain. The waveform captured in time domain has a total time length of 122 ns. The sampling rate of the waveform is 63.5 ps which gives 1920 samples per waveform. The radio has a bandwidth of 4.2 GHz and the center frequency is 5.1 GHz. The radio transmits 9.6 million pulses per second on an average, implying that multipath spreads of more than 100 ns can be observed unambiguously. The antenna used in the radio are omni-directional, non-dispersive antenna. Time domain UWB measurements were made using the software that acts as a interface between UWB radio and user. The minimum distance between the transmitter and receiver should be 3.2 meters and the minimum distance the antenna should be placed above the ground should be 1 meter.

3.1.3 Spatial Measurement Setup

Figure 3.3 shown below is the spatial measurement setup used for the data collection. At each indoor location (receiver position) in any given area, measurements were taken at 25 different measuring points using a 5×5 squared grid. The distance between each spatial measuring points is 15cm, which corresponds to almost 2.5 times the wavelength of the center frequency. The transmitter and the receiver were placed at a optimal height of 1

meter.

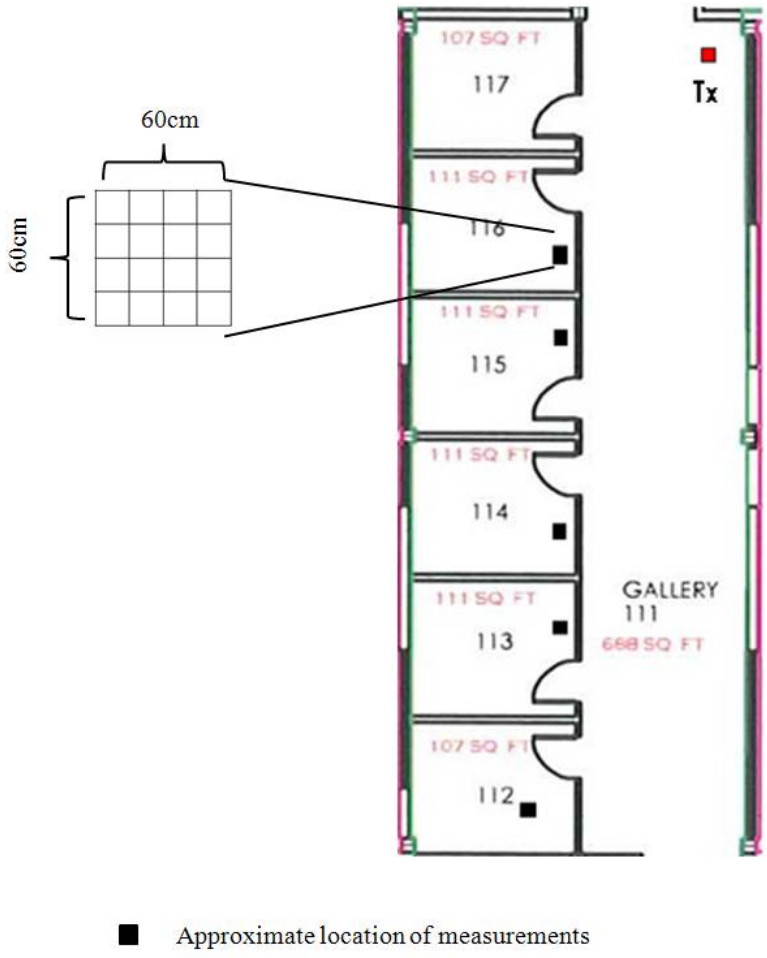

Figure 3.3: Spatial Measurement Setup

3.2 Database

Using the the above mentioned experimental setup, the experiments were conducted to build a large database in order to achieve the first goal of this research. At each location, measurements were made at two raw datarates of 75 kbps and 600 kbps. At each indoor (except LOS measurement for pathloss) location, 25 measurements were made using the

5×5 grid. There were a total of 43 indoor measuring locations across 7 different areas which totals to 2150 PDPs. The database also had 172 LOS PDPs from 28 measurement locations in Galley 340 and 58 measuring locations in Intramural field taken at two different datarates. All components of the database are summarized in table 3.1.

Table 3.1: Database Summary

Areas	No. of Locations	No. of Measurements
CAT 117	4	200
CAT 221	4	200
Gallery 340	9	450
Corridor 352	4	200
Gallery 111	15	750
Corridor 103	2	100
Belk 362	5	250
Intramural field, Gallery 340 (LOS)	86	172

CHAPTER 4: RESULTS

4.1 Data Processing

All the measured data were processed before the data were analyzed to arrive at the results. Firstly the DC components in the waveforms induced by the the correlators in the UWB radio were removed. At any given location if a waveform could not be captured in the measuring grid due to shadowing effect, the record was set to zero initially. All those empty records were removed from the database, resulting a total number of 2137 measurements used for analysis.

The waveform duration of 122 ns was divided into 240 bins with a bin size of 0.5 ns each. For each of the waveform the power is calculated at each bin to arrive at the PDP. Once the PDP was calculated, threshold of 3dB down from the peak was set to calculate the Mean delay and RMS delay spread. The delay characteristics of all the areas were calculated and threshold were set to remove the outliers from the database. Thresholds of -44dB for 75 kbps data and -35db for 600 kbps were set to exclude the effects of noise power from the PDP before calculating the ensemble mean of PDP.

4.2 Analysis Results

The processed database was analyzed to characterize the indoor and outdoor pathloss model, amplitude decay and time dispersion characteristics. The results of all the considerations are summarized below.

4.2.1 Pathloss Model

The pathloss of the LOS UWB signal at varying distance was calculated in outdoor (figure 4.1) and indoor (figure 4.2) environments. The pathloss from the reference distance of 3.2m is calculated at each measuring point i.e., at every meter away from the transmitter. Analysis of the data shows that both the sets of data can be modeled with two distinct line with different slopes. The break point for the outdoor data was 35m and for the indoor environment was found to be 16m. We suspect the reason for the large difference in break point distance between indoor and outdoor environment should be due to large number of multipaths arriving at the receiver in indoor environment.

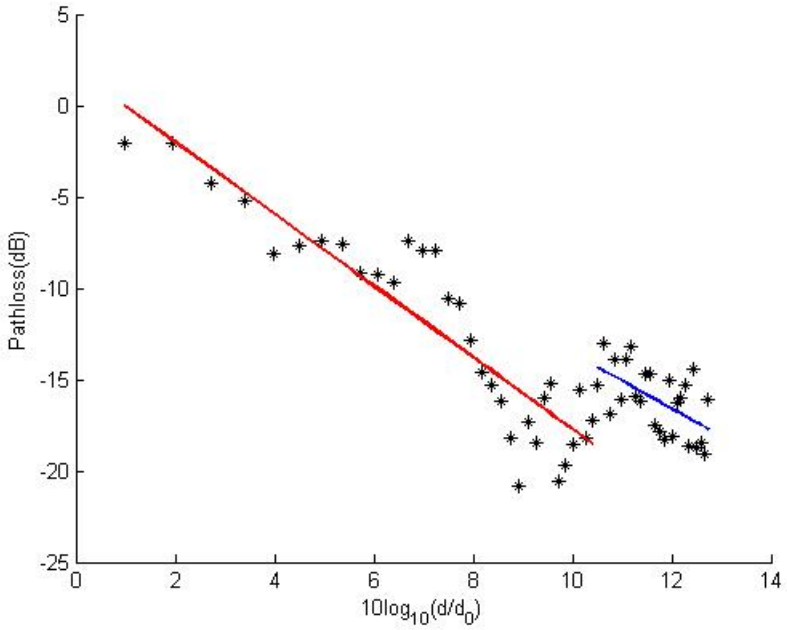

Figure 4.1: Scatter plot of pathloss with regression fit against the logarithm of distance for outdoor data

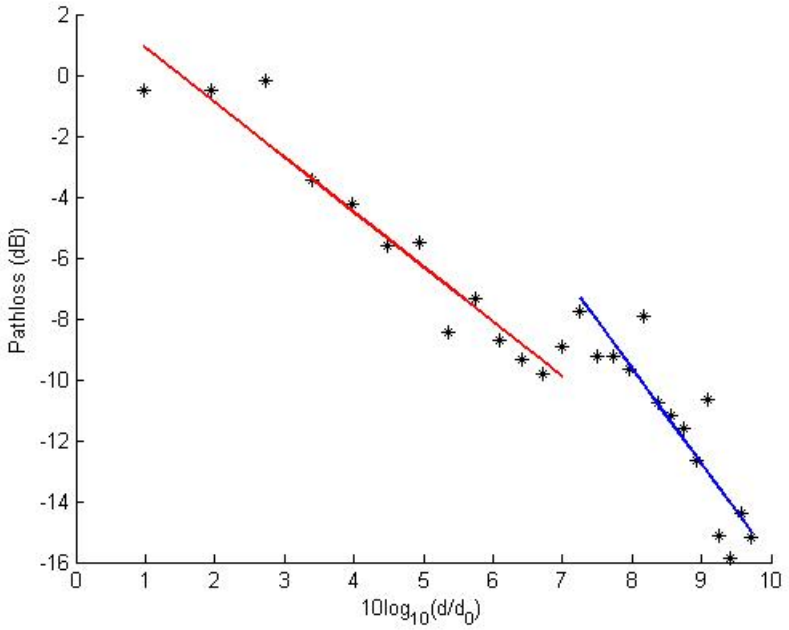

Figure 4.2: Scatter plot of pathloss with regression fit against the logarithm of distance for indoor data

The figures also has the regression fit for the data points. The Pathloss equation was arrived using the regression fit of the data points. The equitation for the outdoor data is given by (4.1) and for the indoor data it is given by (4.2).

$$PL_o = \begin{cases} -19.65 \cdot log_{10}(d/d_0) + 1.9, & d \leq 35m \\ -15.13 \cdot log_{10}(d/d_0) + 1.56, & d > 35m \end{cases} \tag{4.1}$$

$$PL_i = \begin{cases} -17.9 \cdot log_{10}(d/d_0) + 2.69, & d \leq 16m \\ -31.25 \cdot log_{10}(d/d_0) + 15.34, & d > 16m \end{cases} \tag{4.2}$$

4.2.2 Amplitude Decay Characteristics

The distribution of power between the measuring points in the grid at a given location is attributed to small scale fading. Figure 4.3 shows PDP calculated form the 25 measure-

ments made at location B in Belk 362 at a datarate of 75 kbps. The linear PDP decays exponentially, verifying the exponential model proposed by Cassioli *et.al*, based on which this research work was conducted. The Normalized PDP is transformed to logarithmic scale and is shown in figure 4.4, where it is evident that the amplitude delay in logarithmic scale is linear.

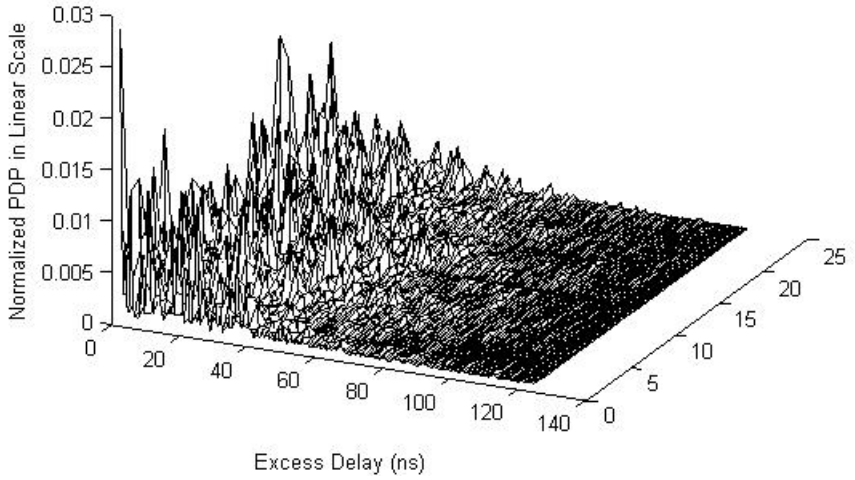

Figure 4.3: Normalized PDP in Linear Scale For Belk 362 - B - 75 kbps

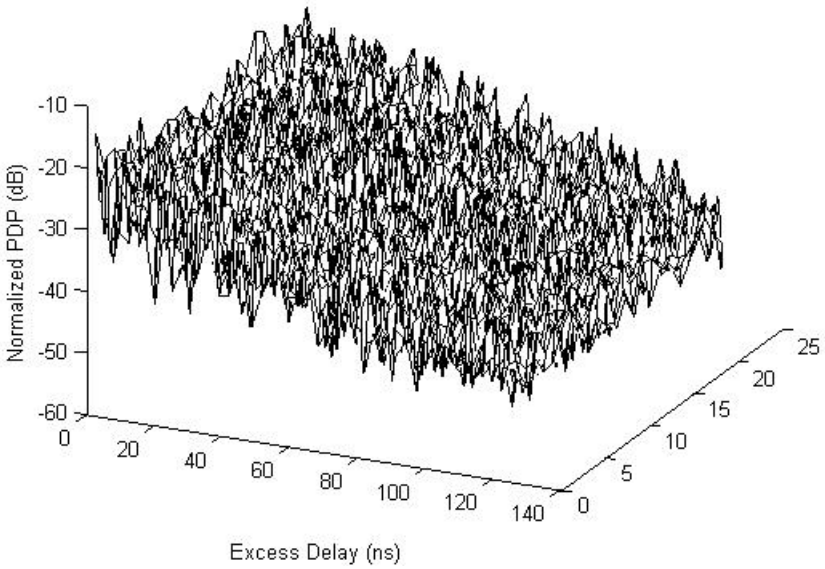

Figure 4.4: Normalized PDP in Log Scale For Belk 362 - B - 75 kbps

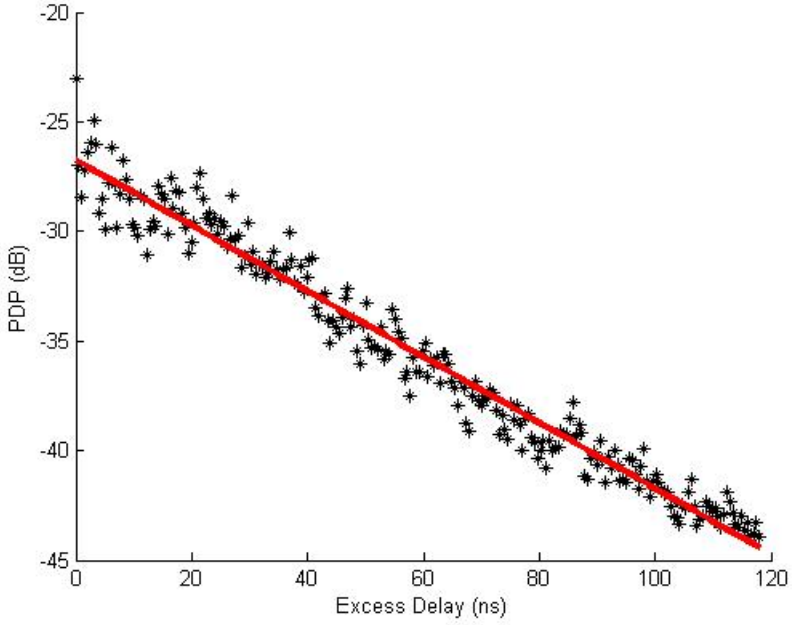

Figure 4.5: Scatter Plot of Ensemble Mean of PDP For Belk 362 - B - 75 kbps

Figure 4.5 shows the scatter plot of the ensemble mean of PDP in log scale and the best fit line is also shown. The coefficients of the polynomial of the best fit line is extracted to arrive at the decay constant of the exponential function. The coefficients of the polynomial of the form $y = ax + b$ for all locations are summarized in table 4.1. The list of figures shown below is the PDP in linear, log scales and the ensemble mean of the PDPs for an exemplary location across different areas representing different environments and layouts.

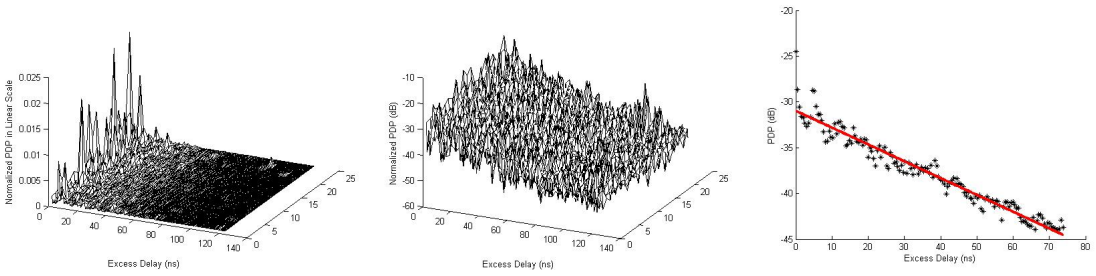

(a) Normalized PDP (b) PDP in Log scale (c) Ensemble Mean of PDP

Figure 4.6: Gallery 340 - 338 - 75 kbps

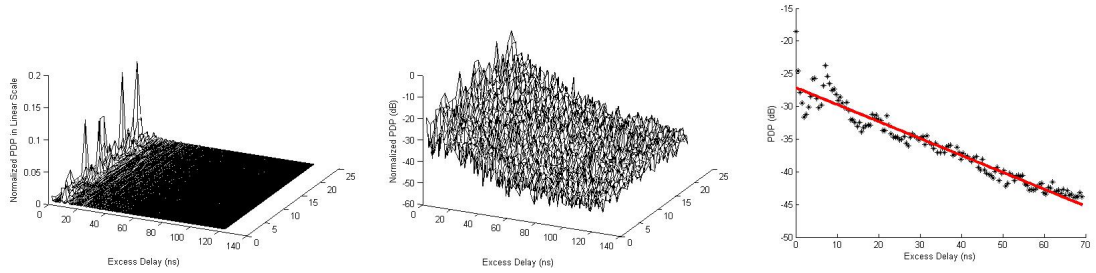

(a) Normalized PDP (b) PDP in Log scale (c) Ensemble Mean of PDP

Figure 4.7: Gallery 111 - 116 - 75 kbps

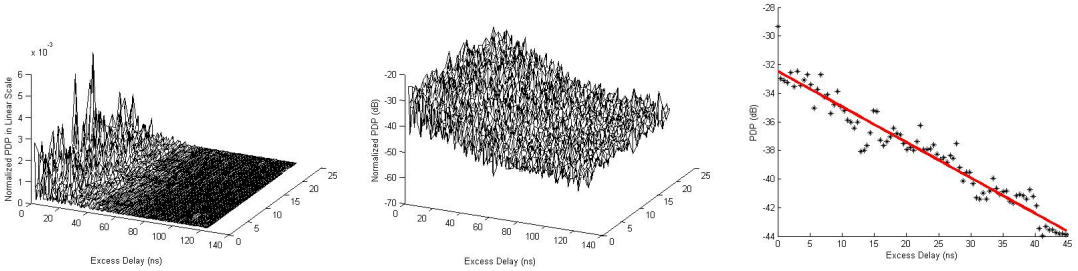

(a) Normalized PDP (b) PDP in Log scale (c) Ensemble Mean of PDP

Figure 4.8: Corridor 103 - 105A - 75 kbps

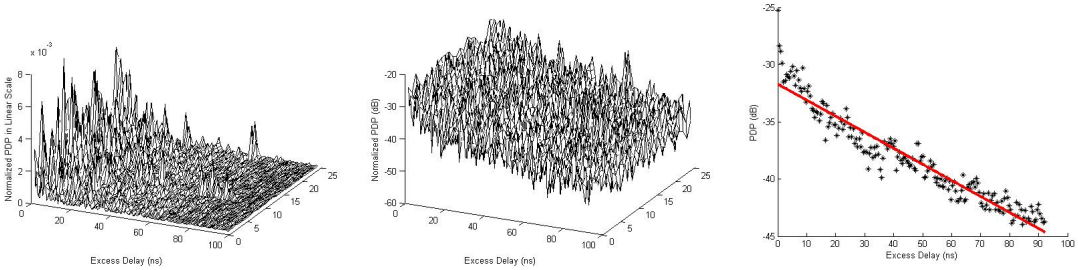

(a) Normalized PDP (b) PDP in Log scale (c) Ensemble Mean of PDP

Figure 4.9: Corridor 352 - 364 - 75 kbps

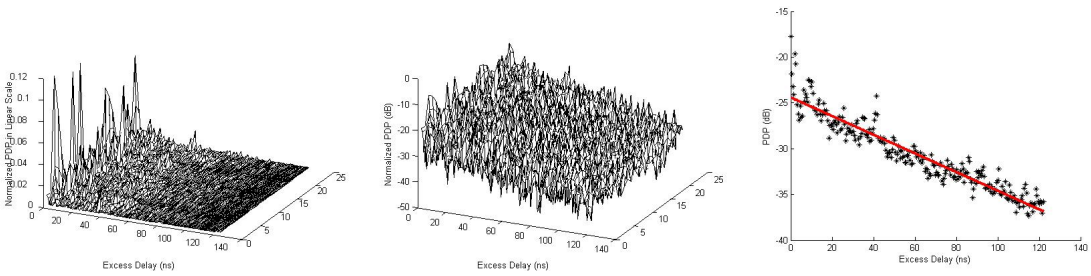

(a) Normalized PDP (b) PDP in Log scale (c) Ensemble Mean of PDP

Figure 4.10: Cat 117 - D - 75 kbps

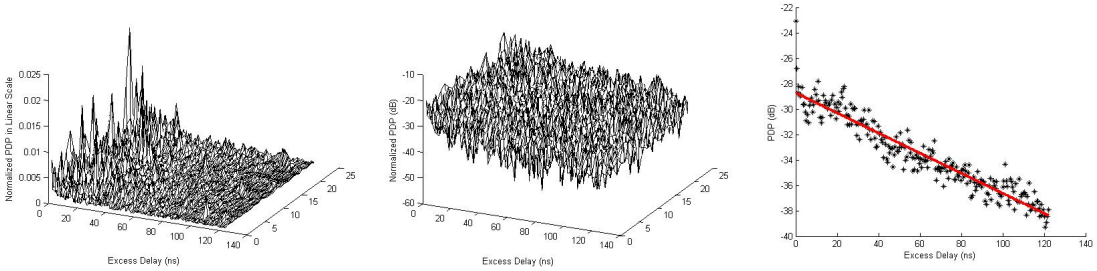

(a) Normalized PDP (b) PDP in Log scale (c) Ensemble Mean of PDP

Figure 4.11: Cat 221 - D - 75 kbps

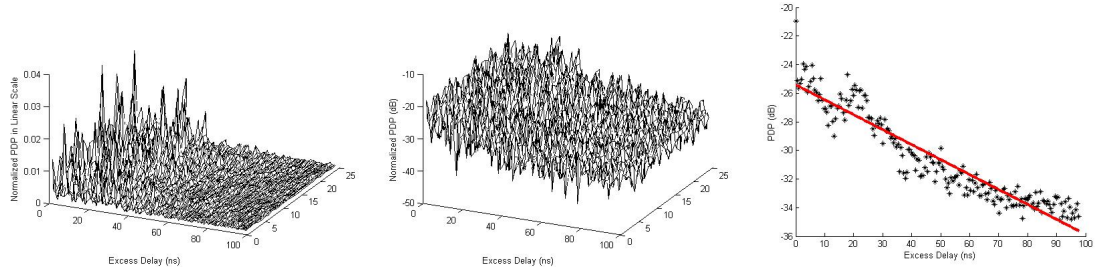

(a) Normalized PDP (b) PDP in Log scale (c) Ensemble Mean of PDP

Figure 4.12: Belk362 - 2 - 600 kbps

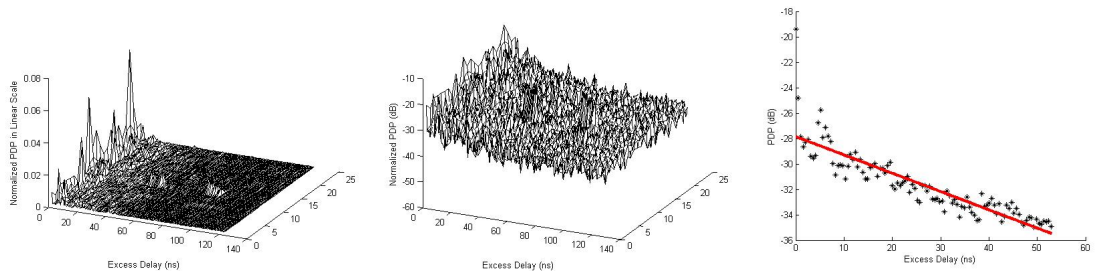

(a) Normalized PDP (b) PDP in Log scale (c) Ensemble Mean of PDP

Figure 4.13: Gallery 340 - 338 - 600 kbps

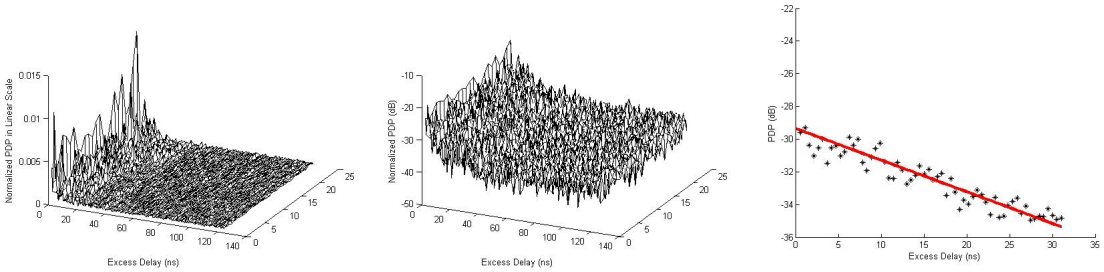

(a) Normalized PDP (b) PDP in Log scale (c) Ensemble Mean of PDP

Figure 4.14: Gallery 111 - 109-A - 600 kbps

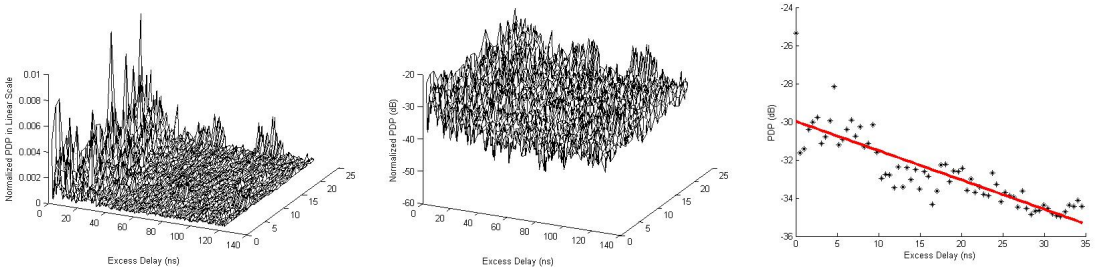

(a) Normalized PDP (b) PDP in Log scale (c) Ensemble Mean of PDP

Figure 4.15: Corridor 103 - 105A - 600 kbps

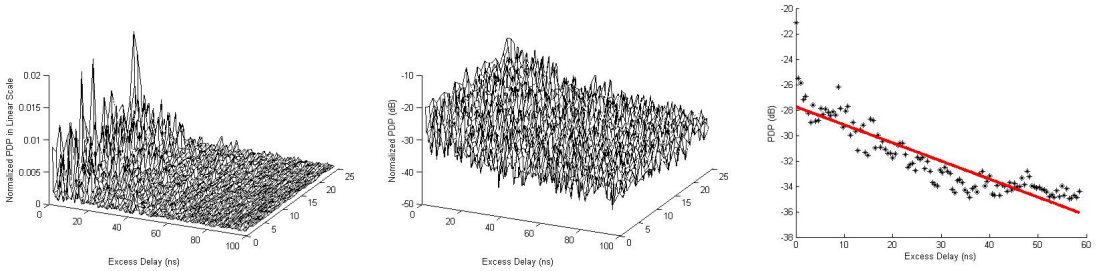

(a) Normalized PDP (b) PDP in Log scale (c) Ensemble Mean of PDP

Figure 4.16: Corridor 352 - 364 - 600 kbps

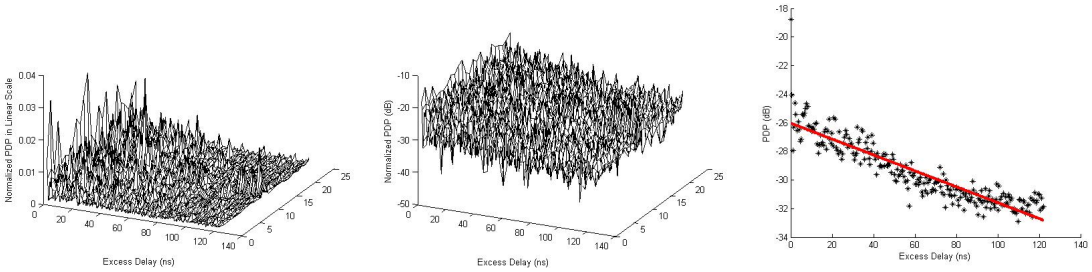

(a) Normalized PDP (b) PDP in Log scale (c) Ensemble Mean of PDP

Figure 4.17: Cat 117 - B - 600 kbps

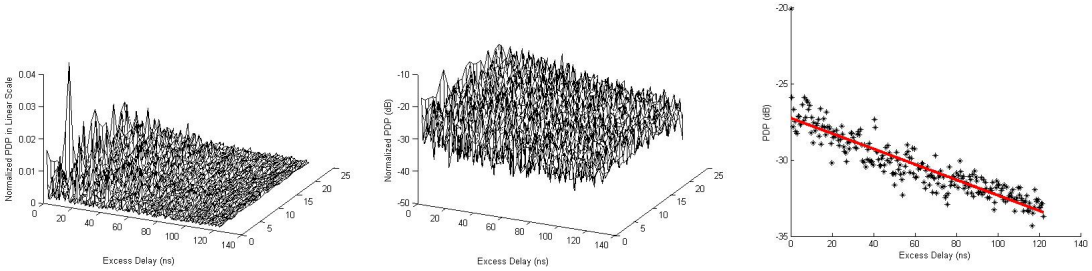

(a) Normalized PDP (b) PDP in Log scale (c) Ensemble Mean of PDP

Figure 4.18: Cat 221 - B - 600 kbps

Table 4.1: Summary of regression fit coefficients for all locations

Area	Location	75 kbps		600 kbps	
		a	b	a	b
Belk 362	A	-0.07688402	-29.229475	-0.063566715	-26.53784
	B	-0.076573647	-26.684724	-0.053448255	-25.376404
	C	-0.071552248	-28.200315	-0.052367026	-20.513267
	D	-0.080855984	-27.493865	-0.053526903	-25.64026
	E	-0.10147818	-20.672948	-0.062177615	-20.339937
Cat117	A	-0.052608089	-24.35299	-0.029975736	-22.794344
	B	-0.045061118	-27.888578	-0.028384466	-26.01432
	C	-0.047002324	-26.239633	-0.031695221	-23.472071
	D	-0.05206573	-24.36504	-0.031588484	-22.616172
Cat221	A	-0.042437231	-26.439634	-0.027891316	-23.685783
	B	-0.039169865	-29.722483	-0.0258214	-27.2449
	C	-0.046277997	-27.75239	-0.030858148	-25.358713
	D	-0.04035086	-28.697975	-0.025980354	-25.763493
Corr 103	105A	-0.12806845	-32.336071	-0.079338417	-29.908606
	106	-0.12653072	-35.728455	-0.07896955	-32.070694
Corr352	360	-0.087036546	-26.836199	-0.042366867	-26.108314
	362	-0.067116767	-32.238773	-0.085646077	-26.61555
	364	-0.071726958	-31.654459	-0.072974667	-27.683932
	365	-0.095612708	-30.754707	-0.084731085	-26.474909
Gallery111	108-A	-0.1724061	-30.241432	-0.13642008	-27.098162
	109-A	-0.15145751	-32.236436	-0.099963928	-29.269896
	110-A	-0.13853955	-31.386053	-0.12346584	-27.986055
	112-A	-0.15236256	-30.517483	-0.12602251	-27.670229
	113-A	-0.13651479	-27.703972	-0.071508699	-26.542625
	114-A	-0.14243082	-26.986843	-0.10905201	-24.960485
	115-A	-0.12952058	-31.207749	-0.10639457	-28.373426
	116-A	-0.11816677	-31.38683	-0.097737167	-28.227044
	117-A	-0.14619999	-33.103642	-0.15991174	-28.426619
	109-B	-0.18541755	-35.034117	-0.12943369	-31.140382
	110-B	-0.17681699	-34.991903	-0.11801407	-31.260971
	112-B	-0.2062777	-35.524972	-0.094311388	-32.273006
	113-B	-0.13775411	-33.911398	-0.10815772	-29.536122
	114-B	-0.14909503	-31.442861	-0.11292594	-28.057529
	116-B	-0.13277032	-27.004592	-0.06071579	-26.481807
Gallery340	339	-0.1237511	-35.557005	-0.088902232	-31.51258
	338	-0.13153051	-32.72344	-0.098488569	-29.711863
	337	-0.12373742	-33.649932	-0.091252524	-30.305768
	336	-0.098384442	-35.372304	-0.066590446	-31.946137
	335	-0.10355074	-29.217068	-0.077612125	-26.58021
	334	-0.094974287	-30.219785	-0.073089883	-27.235632
	333	-0.096687627	-30.148989	-0.072378221	-27.405124
	332	-0.094046999	-30.893631	-0.073940355	-27.795089
	331	-0.10133801	-32.309333	-0.077721732	-29.004548

4.2.3 Time Dispersion Characteristics

On analyzing the Large scale NLOS data i.e., data obtained by lumping all the NLOS data from a discrete area, it was found that the time dispersion parameters such as mean excess delay and RMS delay spread follow the Weibull distribution. The statistical property of the time dispersion parameters is a unique finding from this research. Weibull distribution is type III extreme value distribution and the probability distribution function of the Weibull distribution is given by

$$f(x;\lambda,k) = \begin{cases} \frac{k}{\lambda}\left(\frac{x}{\lambda}\right)^{k-1} e^{-(x/\lambda)^k} & x \geq 0, \\ 0 & x < 0, \end{cases} \tag{4.3}$$

where $k > 0$ is the shape factor and $\lambda > 0$ is the scale factor. Figure 4.19 shows the Weibull pdf with different k and λ values.

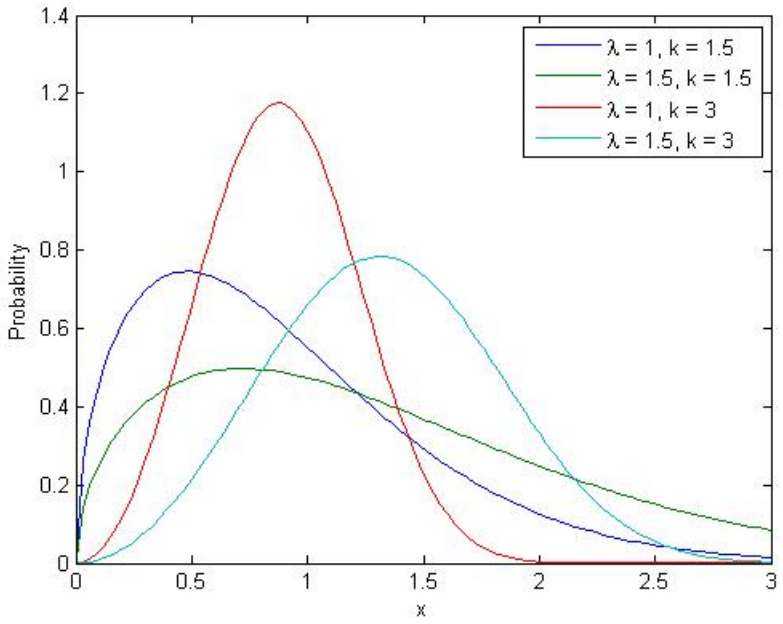

Figure 4.19: Weibull pdf for different λ and k values

Figure 4.20 shows the probability plot for the Mean delay data calculated for all

the measurements from Belk 362. On analyzing the data from all the areas, it is evident that both time dispersion parameters namely the mean and RMS delay spreads fit well with Weibull pdf for most of the areas. The areas which the data does not fit quite well are the two laboratories in CAT building - CAT 117 and CAT 221. Both CAT 221 and 117 are the areas chosen to represent industrial environment. Figure 4.21 shown is the Weibull pdf along with the histogram of the mean excess delay from Belk 362 to confirm that the data follow Weibull distribution. Also shown below are probability plots and pdf plots for mean and RMS delay spreads across all the areas and at all datarates. .

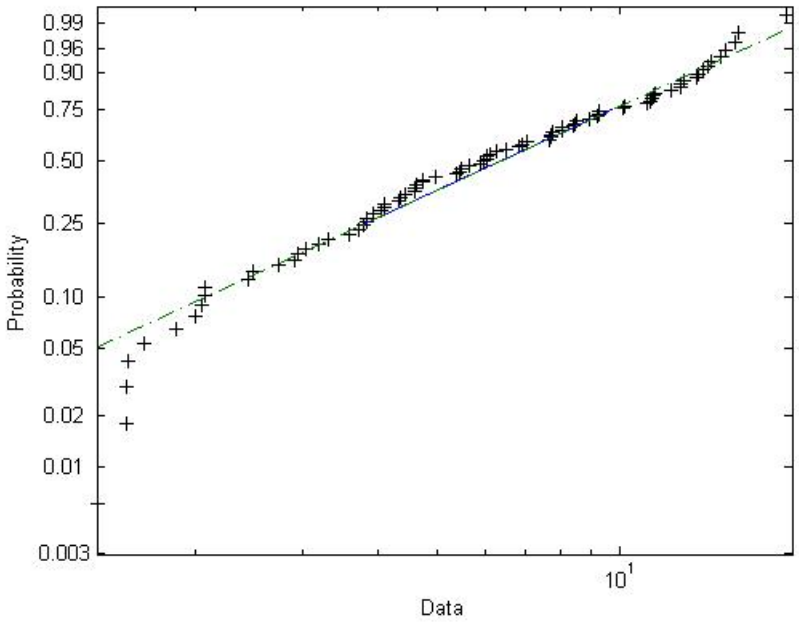

Figure 4.20: Weibull Probability plot for Mean Delay - Belk 362 - 75 kbps

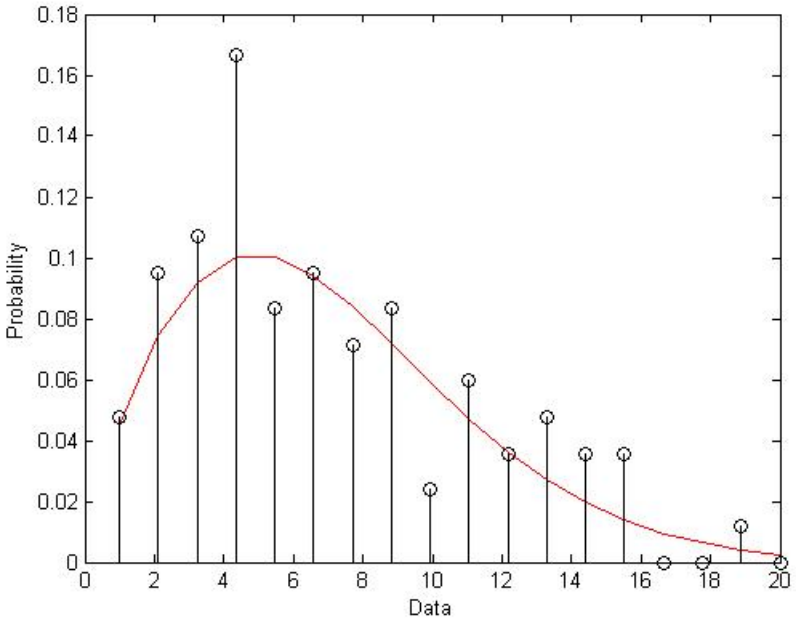

Figure 4.21: Weibull pdf and histogram of data for Mean Delay - Belk 362 - 75 kbps

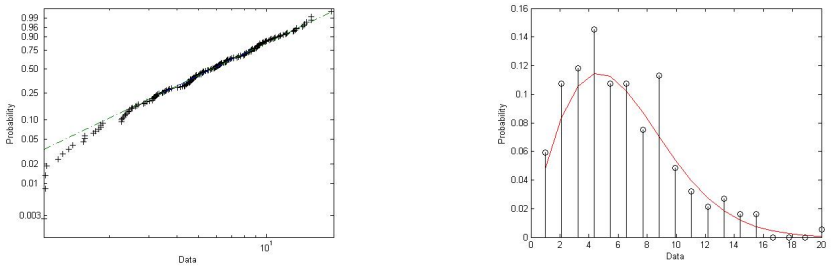

(a) Probability Plot (b) Weibull pdf

Figure 4.22: Gallery 340 - 75 kbps - Mean Delay

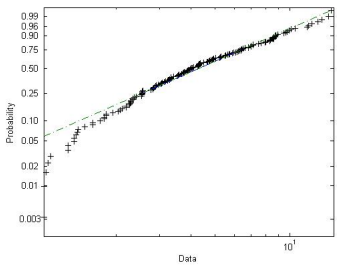

(a) Probability Plot

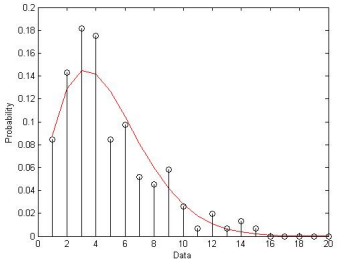

(b) Weibull pdf

Figure 4.23: Gallery 340 - 75 kbps - RMS Delay

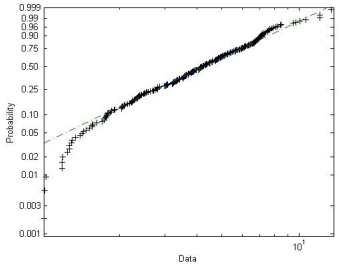

(a) Probability Plot

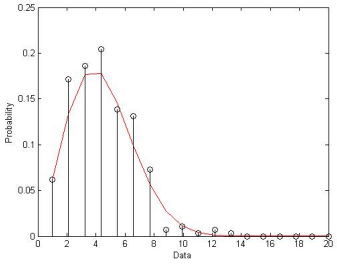

(b) Weibull pdf

Figure 4.24: Gallery 111 - 75 kbps - Mean Delay

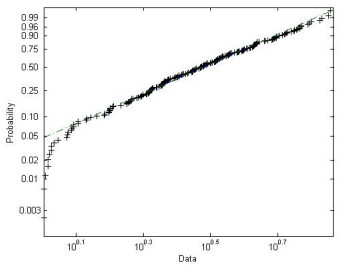

(a) Probability Plot

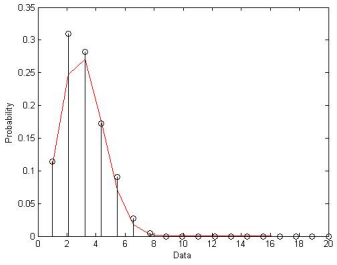

(b) Weibull pdf

Figure 4.25: Gallery 111 - 75 kbps - RMS Delay

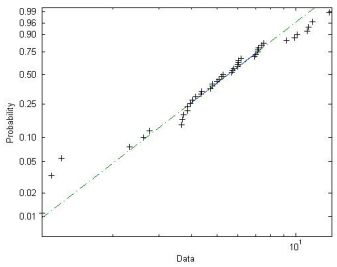

(a) Probability Plot

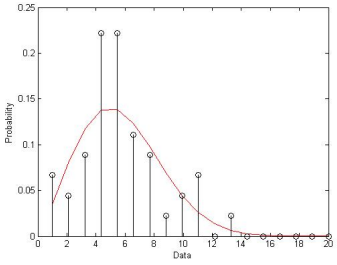

(b) Weibull pdf

Figure 4.26: Corridor 103 - 75 kbps - Mean Delay

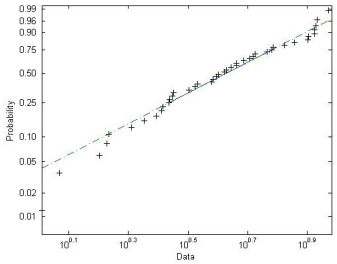

(a) Probability Plot

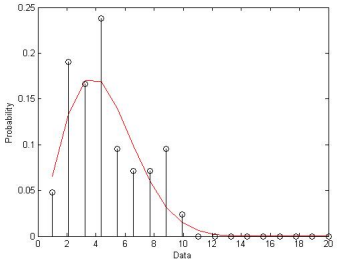

(b) Weibull pdf

Figure 4.27: Corridor 103 - 75 kbps - RMS Delay

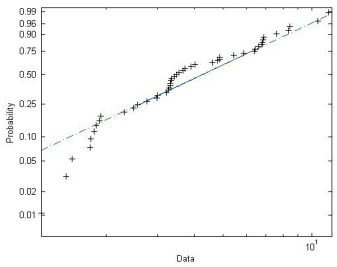

(a) Probability Plot

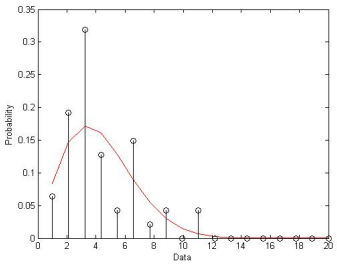

(b) Weibull pdf

Figure 4.28: Corridor 352 - 75 kbps - Mean Delay

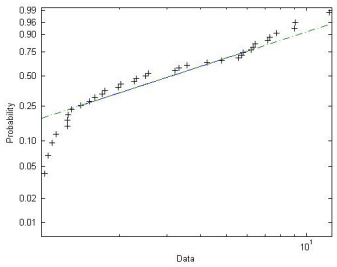

(a) Probability Plot

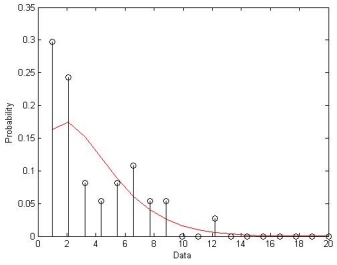

(b) Weibull pdf

Figure 4.29: Corridor 352 - 75 kbps - RMS Delay

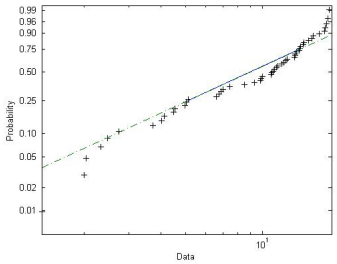

(a) Probability Plot

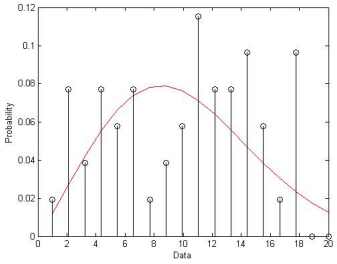

(b) Weibull pdf

Figure 4.30: Cat 117 - 75 kbps - Mean Delay

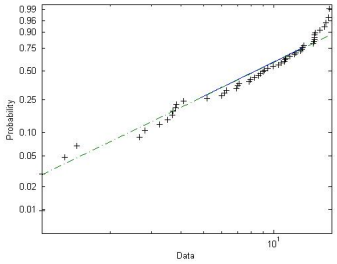

(a) Probability Plot

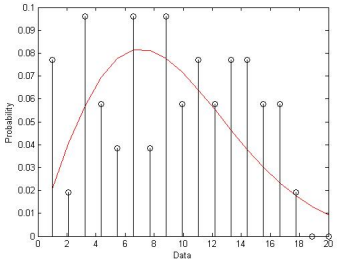

(b) Weibull pdf

Figure 4.31: Cat 117 - 75 kbps - RMS Delay

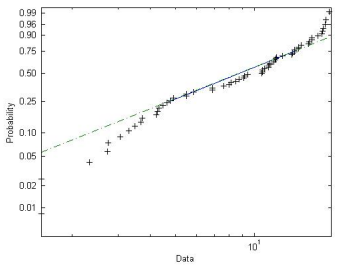

(a) Probability Plot

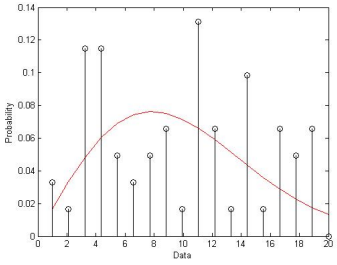

(b) Weibull pdf

Figure 4.32: Cat 221 - 75 kbps - Mean Delay

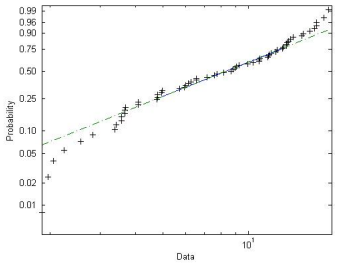

(a) Probability Plot

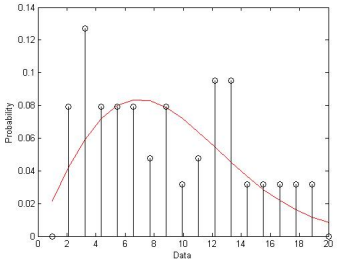

(b) Weibull pdf

Figure 4.33: Cat 221 - 75 kbps - RMS Delay

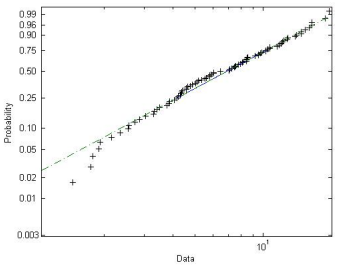

(a) Probability Plot

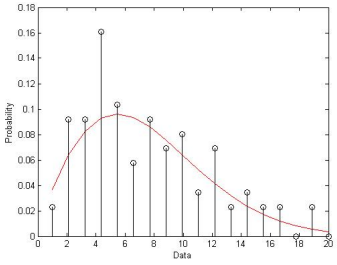

(b) Weibull pdf

Figure 4.34: Belk362 - 600 kbps - Mean Delay

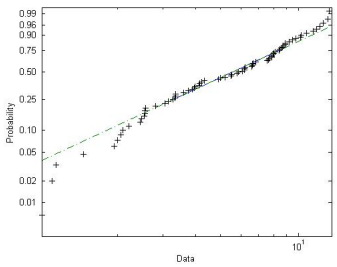

(a) Probability Plot

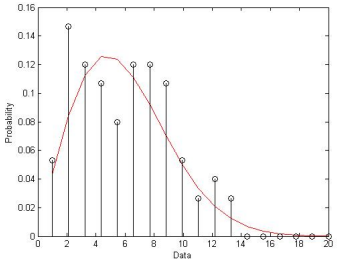

(b) Weibull pdf

Figure 4.35: Belk362 - 600 kbps - RMS Delay

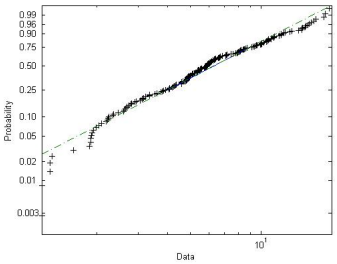

(a) Probability Plot

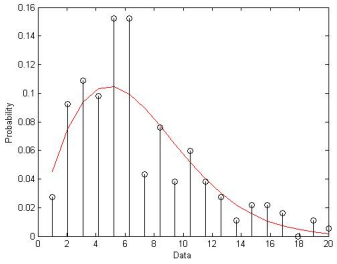

(b) Weibull pdf

Figure 4.36: Gallery 340 - 600 kbps - Mean Delay

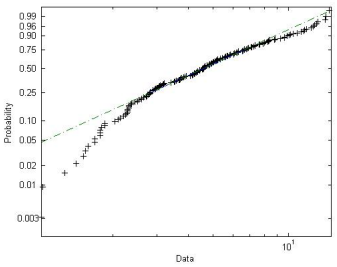

(a) Probability Plot

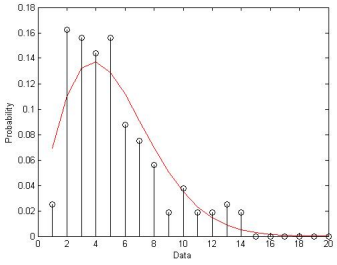

(b) Weibull pdf

Figure 4.37: Gallery 340 - 600 kbps - RMS Delay

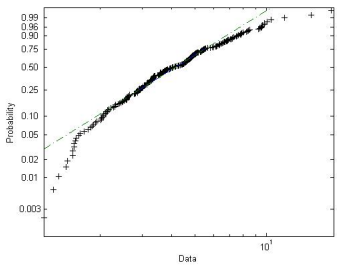

(a) Probability Plot

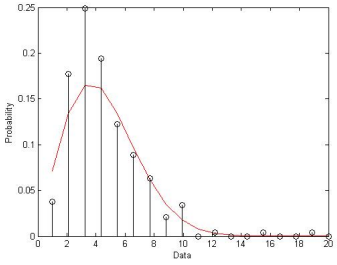

(b) Weibull pdf

Figure 4.38: Gallery 111 - 600 kbps - Mean Delay

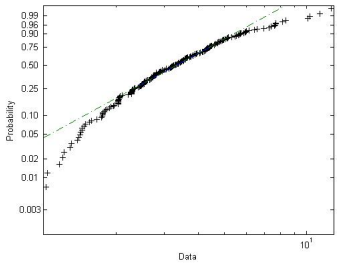

(a) Probability Plot

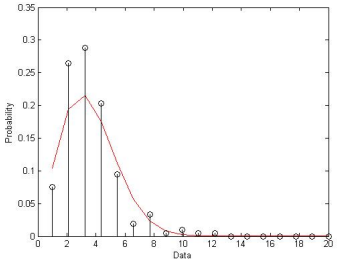

(b) Weibull pdf

Figure 4.39: Gallery 111 - 600 kbps - RMS Delay

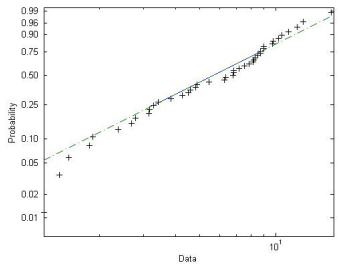

(a) Probability Plot

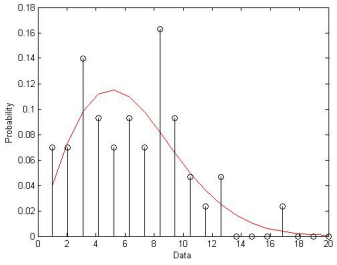

(b) Weibull pdf

Figure 4.40: Corridor 103 - 600 kbps - Mean Delay

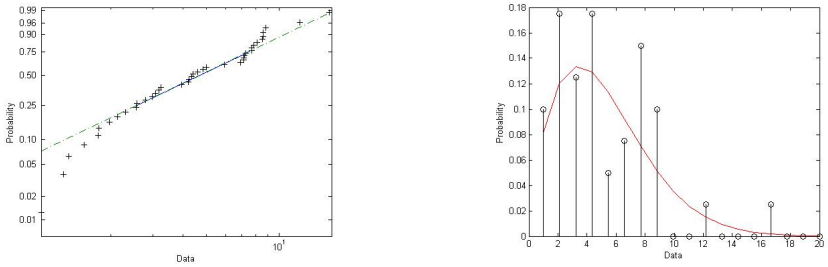

(a) Probability Plot (b) Weibull pdf

Figure 4.41: Corridor 103 - 600 kbps - RMS Delay

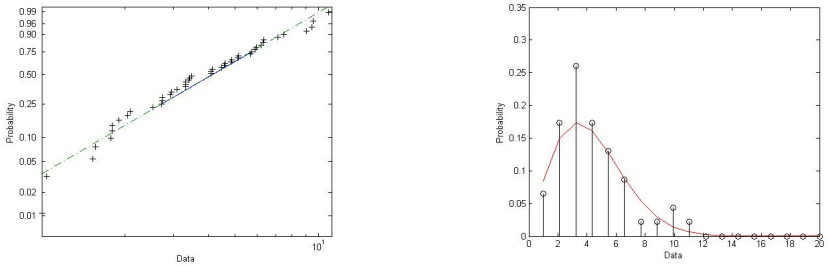

(a) Probability Plot (b) Weibull pdf

Figure 4.42: Corridor 352 - 600 kbps - Mean Delay

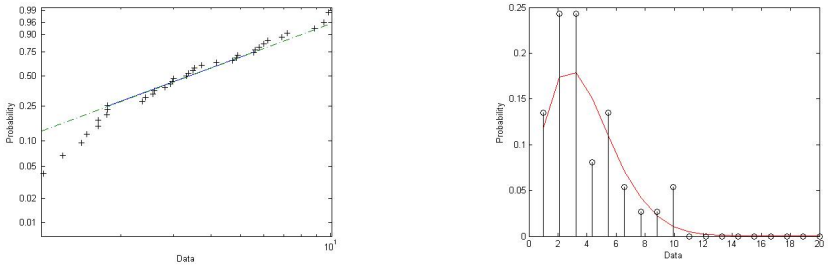

(a) Probability Plot (b) Weibull pdf

Figure 4.43: Corridor 352 - 600 kbps - RMS Delay

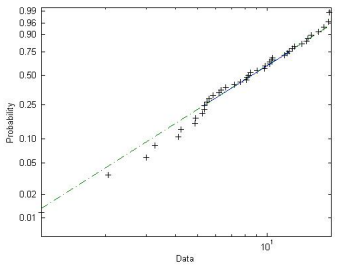

(a) Probability Plot

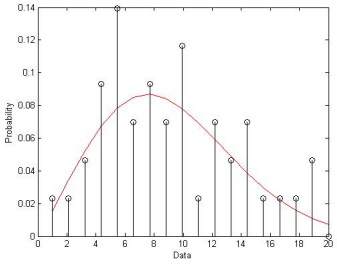

(b) Weibull pdf

Figure 4.44: Cat 117 - 600 kbps - Mean Delay

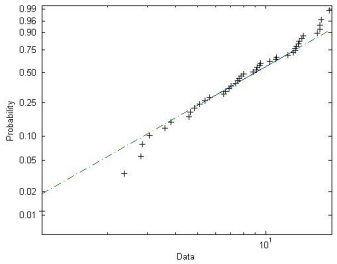

(a) Probability Plot

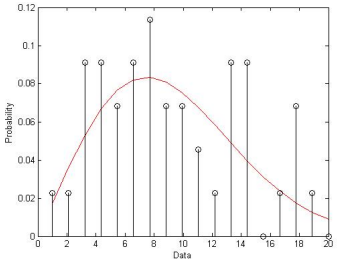

(b) Weibull pdf

Figure 4.45: Cat 117 - 600 kbps - RMS Delay

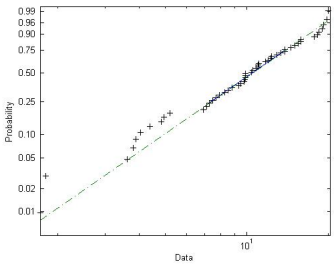

(a) Probability Plot

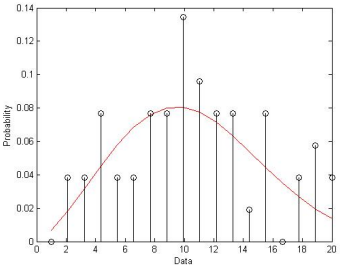

(b) Weibull pdf

Figure 4.46: Cat 221 - 600 kbps - Mean Delay

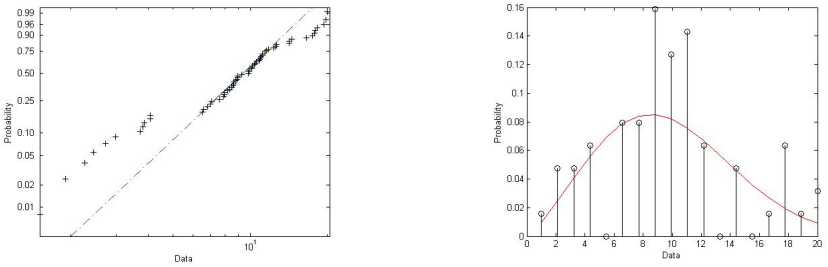

(a) Probability Plot (b) Weibull pdf

Figure 4.47: Cat 221 - 600 kbps - RMS Delay

The parameters of the Weibull distribution λ and k are extracted for the data sets from all the areas using a 95% confidence interval. In tables below the parameters of the Weibull distribution with a lower and upper bounds of the 95% confidence interval is summarized across all the areas. The values in the table clearly show that each environment and layout has different parameter values. CAT 221 and 117 which represent the industrial environment have almost same values. Among the academic environments, all of the four different layouts have slightly different values. Variations were observed for Gallery 111 and Gallery 340 despite their similar layouts. We suspect that the variation between Gallery 111 and Gallery 340 is due to the presence of huge glass panels in the side of the Gallery 111. The presence of glass panel made the UWB waves diffract rather than reflect. The large glass panels also increased the possibility of introducing interference from external sources and thus caused the UWB signal to behave differently.

Table 4.2: Weibull Parameters Summary - Mean Delay - 75 kbps

Area	λ	k	95 % Confidence Interval		
				λ	k
Belk362	7.8832	1.7612	Lower	6.9338	1.4904
			Upper	8.9625	2.0812
Cat117	11.3757	2.1397	Lower	9.9593	1.7014
			Upper	12.9935	2.6908
Cat221	11.1713	1.9843	Lower	9.7806	1.6145
			Upper	12.7597	2.4388
Corr 103	6.5179	2.2046	Lower	5.6675	1.7647
			Upper	7.4959	2.7542
Corr352	4.9142	1.954	Lower	4.2082	1.5777
			Upper	5.7386	2.4202
Gallery111	5.0296	2.207	Lower	4.7525	2.0176
			Upper	5.3229	2.414
Gallery340	7.1068	1.8474	Lower	6.5464	1.6538
			Upper	7.7152	2.0638

Table 4.3: Weibull Parameters Summary - Mean Delay - 600 kbps

Area	λ	k	95% Confidence Interval		
				λ	k
Belk362	8.4254	1.8241	Lower	7.46	1.5494
			Upper	9.5158	2.1474
Cat117	10.2609	2.1159	Lower	8.8421	1.6705
			Upper	11.9073	2.6799
Cat221	11.9777	2.3652	Lower	10.6151	1.9023
			Upper	13.5151	2.9408
Corr 103	7.305	1.944	Lower	6.213	1.5339
			Upper	8.5889	2.4638
Corr352	4.8777	1.9555	Lower	4.1716	1.5708
			Upper	5.7034	2.4345
Gallery111	5.1483	2.0145	Lower	4.8146	1.8412
			Upper	5.5051	2.2041
Gallery340	7.6573	1.7946	Lower	7.032	1.6084
			Upper	8.3382	2.0023

Table 4.4: Weibull Parameters Summary - RMS Delay - 75 kbps

Area	λ	k	95% Confidence Interval		
				λ	k
Belk362	5.9895	1.5934	Lower	5.1434	1.3367
			Upper	6.9748	1.8994
Cat117	10.2999	1.9425	Lower	8.897	1.5461
			Upper	11.924	2.4405
Cat221	10.0839	1.948	Lower	8.8226	1.5968
			Upper	11.5256	2.3765
Corr 103	5.1105	2.1069	Lower	4.3913	1.6634
			Upper	5.9474	2.6686
Corr352	4.1847	1.4225	Lower	3.2911	1.1116
			Upper	5.3209	1.8202
Gallery111	3.5363	2.4377	Lower	3.3393	2.2042
			Upper	3.745	2.6959
Gallery340	5.4174	1.7335	Lower	4.919	1.5396
			Upper	5.9664	1.9518

Table 4.5: Weibull Parameters Summary - RMS Delay - 600 kbps

Area	λ	k	95% Confidence Interval		
				λ	k
Belk362	6.7678	1.9932	Lower	6.0046	1.6634
			Upper	7.628	2.3883
Cat117	10.4206	2.0414	Lower	8.9481	1.6104
			Upper	12.1354	2.5878
Cat221	11.0074	2.2741	Lower	9.8202	1.8721
			Upper	12.3381	2.7623
Corr 103	5.8242	1.6936	Lower	4.7995	1.3373
			Upper	7.0676	2.1446
Corr352	4.41	1.7843	Lower	3.642	1.3974
			Upper	5.34	2.2782
Gallery111	4.0859	2.1	Lower	3.8171	1.9098
			Upper	4.3735	2.3092
Gallery340	5.8978	1.8229	Lower	5.3897	1.623
			Upper	6.4538	2.0474

CHAPTER 5: CONCLUSION AND FUTURE WORK

Thus the database which contains different variables like environment, layout, and raw datarate was established from the measurement campaign. The experiment was designed to include all the variables to increase the credibility of the research and have inclusiveness of different scenarios. Upon building the database, data processing was done to weed out the bad data. Initial analysis and investigation of the data verified the exponential model and confirmed that our UWB channel does have a exponential decay amplitude characteristics. On analyzing the data further, it was found that the time dispersion characteristics namely mean excess delay and RMS delay spread follow Weibull distribution across all the areas and layouts. The parameters of the Weibull distribution for all the areas and layouts were extracted and presented. This new finding

For the future work, a complete measurement campaign which includes different types of residential and commercial environment can be done. The research can also be further extended to investigate interference due to narrow band signal and inter symbol interferences.

BIBLIOGRAPHY

[1] T. S. Rappaport, *Wireless communications : principles and practice*, Prentice Hall PTR, Upper Saddle River, N.J., 2002.

[2] M. Z. Win and R. A. Scholtz, "Impulse radio: how it works", *IEEE Communications Letters*, vol. 2, no. 2, pp. 36-38, Feb. 1998.

[3] M. Z. Win and R. A. Scholtz, " On the robustness of ultra-wide bandwidth signals in dense multipath environments", *IEEE Communication Letters*, vol. 2, no. 2, pp. 51-53, 1998.

[4] R. A. Scholtz, R. J. M Cramer, and M. Z. Win, "Evaluation of the propagation characteristics of ultra-wideband communication channels", *IEEE Antennas and Propagation Society International Symposium*, 1998, vol. 2, pp. 626-630.

[5] M. Z Win and R. A. Scholtz, "Ultra-wide bandwidth time-hopping spread-spectrum impulse radio for wireless multiple-access communications", *IEEE Transactions on Communications*, vol. 48, no. 4, pp. 679-689, Apr. 2000.

[6] M. Z. Win and R. A Scholtz, "Characterization of ultra-wide bandwidth wireless indoor channels: a communication-theoretic view", *IEEE Journal on Selected Areas in Communications*, vol. 20, no. 9, pp. 1613-1627, 2002.

[7] W. Hirt, "Ultra-wideband radio technology: overview and future research", *Computer Communications*, vol. 26, no.1, pp. 46-52, 2003.

[8] Y. Liuqing and G. B. Giannakis,"Ultra-wideband communications: an idea whose time has come", *IEEE Signal Processing Magazine*, vol. 21, no. 6, pp. 26-54, 2004.

[9] A. F. Molisch, J. R. Foerster, and M. Pendergrass, "Channel models for ultrawideband personal area networks", *IEEE Wireless Communications*, vol. 10, no. 6, pp. 14-21, 2003.

[10] A. F. Molisch, "Ultrawideband propagation channels-theory, measurement, and modeling", *IEEE Transactions on Vehicular Technology*, vol. 54, no. 5, pp. 1528-1545, 2005.

[11] A. F. Molisch, "Ultra-Wide-Band Propagation Channels", *Proceedings of the IEEE*, vol. 97, no. 2, pp. 353-371, 2009.

[12] D. Cassioli, M. Z. Win, and A. F. Molisch, "The ultra-wide bandwidth indoor channel: from statistical model to simulations", *IEEE Journal on Selected Areas in Communications*, vol. 20, no.6, pp. 1247-1257, Aug. 2002.

[13] B. M. Donlan, D. R. McKinstry, and R. M. Buehrer, "The UWB indoor channel: large and small scale modeling", *IEEE Transactions on Wireless Communications*, vol. 5, no. 10, pp. 2863-2873, 2006.

[14] S. S. Ghassemzadeh, L. J. Greenstein, A. Kavcic, T. Sveinsson, and V. Tarokh, "UWB indoor delay profile model for residential and commercial environments", *IEEE 58th Vehicular Technology Conference*, 2003, vol. 5, pp. 3120-3125.

[15] S. S. Ghassemzadeh, L. J. Greenstein, T. Sveinsson, A. Kavcic, and V. Tarokh, "UWB Delay Profile Models for Residential and Commercial Indoor Environments", *IEEE Transactions on Vehicular Technology*, vol. 54, no. 4, pp. 1235-1244, 2005.

[16] L. J. Greenstein and S. S. Ghassemzadeh, ”Comparing Three Models for UWB Indoor Power Delay Profile”, *40th Annual Conference on Information Sciences and Systems*, 2006, pp. 626-631.

[17] L. J. Greenstein, S. S. Ghassemzadeh, Seung-Chul Hong, and V. Tarokh, ”Comparison study of UWB indoor channel models”, *IEEE Transactions on Wireless Communications*, vol. 6, no. 1, pp. 128-135, 2007.

[18] H. Al-Tamimi and S. M. Al-Qaraawy, ”UWB propagation indoor statistical channel modeling”, *International Colloquium on Computing, Communication, Control, and Management*, 2009, vol. 1, pp. 379-383.

[19] B. Sklar, ”Rayleigh fading channels in mobile digital communication systems .I. Characterization”, *IEEE Communications Magazine*, vol. 35, no. 7, pp. 90-100, Jul. 1997.